Modelling the dispersion of radionuclides in estuarine environments: the Odiel river estuary

R. Periáñez, J. M. Abril

Dpto. Física Aplicada I, E. U. Ingeniería Técnica Agrícola, Universidad de Sevilla, Ctra. Utrera km 1, 41013-Sevilla, Spain

1. Introduction

An estuary is defined as a semi-enclosed coastal body of water which has a free connection with the open sea and in which sea water is mixed with freshwater. Estuaries form the transition from rivers to the sea and present a separate environment, influenced by conditions in the river and in the coastal area. Huge industrial facilities are often located along estuaries, as well as human settlements. Thus, it may be relevant to study contamination in estuaries and to develop models that simulate the dispersion of pollutants so as to assess contamination levels following potential accidental releases from the industries. In particular, this is valid for the case of radioactive contamination, which can be released to the aquatic environment not only from nuclear related industries.

A numerical model to simula te the dispersion of natural radionuclides (^{226}Ra, ^{238}U, ^{232}Th) in an estuary of southwest Spain is presented in this chapter. These radionuclides are released from a phosphate fertilizer processing complex.

1.1. *Physical features of an estuary: selecting a model*

The model used to simulate the dispersion of radionuclides (or any pollutant in general) in an estuarine system will be defined by the time scale in which we are interested (usually interest will focus in simulating tide and wind dispersion during several days or weeks) and by the physical characteristics of the particular estuary: from shape and topography to water circulation.

The different types of estuarine circulation are presented in Fig. 1 (from Postma, 1980). In the absence of tides (Fig. 1a), the river water flows over the sea water due to its lower density. Mixing between fresh and salt water is limited and mainly occurs because of surface waves and tidal currents. Most of the suspended matter supplied by the river settles in the area of contact between the two water masses due to the reduction in the flow velocity which

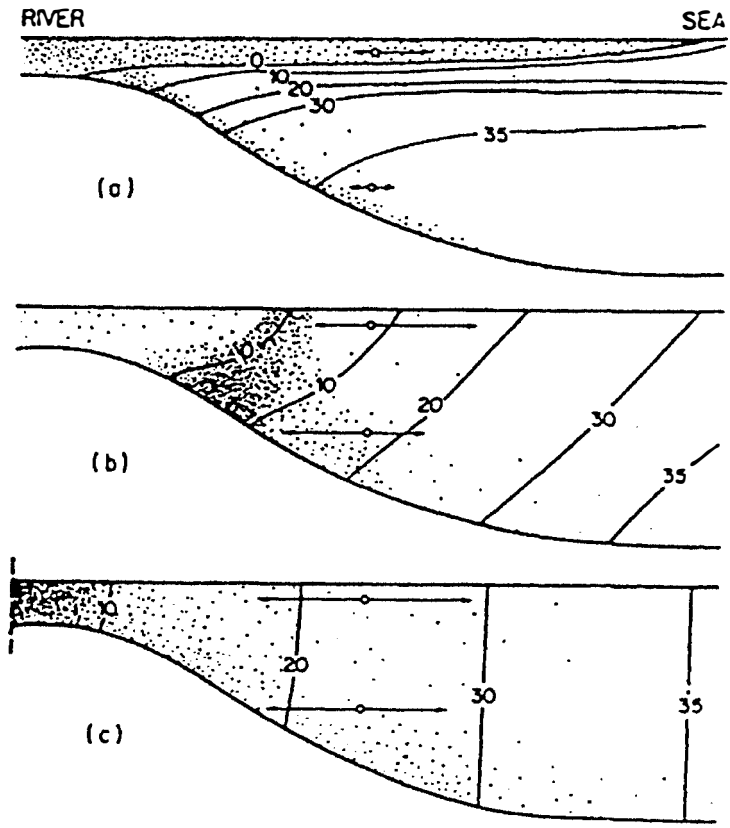

Fig. 1. Circulation in estuaries. Isolines represent salinity, vectors represent the residual currents and points the suspended particles. (a) Non tidal estuary, (b) partially mixed estuary, (c) fully mixed estuary.

usually occurs here. In tidal estuaries, two cases can be distinguished: partially mixed and fully mixed estuaries. In partially mixed estuaries (Fig. 1b) vertical mixing is incomplete and strong vertical density gradients occur. This mixing of the fresh water discharged by the river with the incoming sea water is enhanced by turbulence induced by the tidal current. As a result, there is an entrainment of salt water into the surface seaward flow of the river, and the sea water carried out to sea in this way is replaced by a net residual flow at the bottom, directed up the estuary. The residual current in the surface is outwards because of the river water flowing out, while in the bottom it is inwards to compensate for the outflow of sea water. The place where upstream residual bottom flow and the downstream river flow converge is called the null point. In most estuaries the null point is associated with a turbidity maximum, where the suspended matter load may be as high as 10 kg/m^3. This area of maximum turbidity is due to the transport of sediments by the converging currents and in some cases to the flocculation of river clays because of the sudden increase of salinity. The null point and the turbidity maximum move along the estuary with spring and neap tides and with the periods of high and low river discharge: more inward during spring tides and low river discharge, and outwards during neap tides and high river discharge. In fully mixed estuaries (Fig. 1c), vertical mixing

is virtually complete and the density gradients are horizontal. This occurs where the tides dominate the river outflow.

The particular circulation of the estuary of interest will define the model to be used. If the estuary is fully mixed, a two dimensional depth-averaged model may be enough since there are no vertical gradients of salinity and suspended matter to be resolved. In the cases of non-tidal and partially mixed estuaries, vertical gradients are present, so that the vertical direction must be resolved too, and a fully three dimensional model is required. However, even if the estuary is fully mixed, a three dimensional model may be required to simulate the dispersion of pollutants depending on the water depth and the magnitude of the tidal currents (which will control the magnitude of the vertical diffusion coefficient). Indeed, Prandle et al. (1993) have shown that vertical structure can be of primary concern when typical simulated times are of the order of one month or less. Moreover, the vertical variability is important for such times, even in shallow waters (depth ~ 50 m), if tidal mixing keeps the vertical diffusion coefficient smaller than 10^{-3} m^2/s, a value that can be considered representative of a relatively strong tidal action (Prandle et al., 1993). In the case of narrow estuaries, another option may be to develop a two dimensional XZ model in the longitudinal and vertical directions, thus averaged in the transverse direction, if this is not relevant. This kind of model is often applied in fjords.

1.2. *The Odiel river estuary*

The Odiel river, in southwest Spain, forms a fully mixed estuary, with M_2 being the main tidal constituent. It is shallow (maximum water depth is ~ 10 m) and the flow of the Odiel river is low, typically ranging from 4 m^3/s (dry season) to 100 m^3/s (wet season). A map of the estuary is presented in Fig. 2. It is surrounded by a marsh area and an industrial complex, located at the south of the town of Huelva. The Tinto river joins the Odiel at the Punta del Sebo, and they flow together from this point to the Atlantic Ocean. Due to the low water discharge, mixing between sea and fresh water occurs north of Huelva. Thus, the water of the estuary in the area close to the industrial complex is virtually sea water. This can be seen in Fig. 3, where salinities measured along the estuary (from Periáñez, 1995) are presented.

A phosphate fertilizer processing plant is located in the industrial complex. This plant released part of its wastes directly to the Odiel river. It is well known (Heijde et al., 1988; Laiche & Scott, 1991) that such wastes contain significant amounts of natural radionuclides (U, Th, Ra and their daughters) due to the fact that the phosphate rock, from which phosphoric acid is obtained, may contain U concentrations ranging from 50 to 300 ppm (Laiche & Scott, 1991). During the wet processing of phosphate rock for phosphoric acid production, for instance, 86% of U and 70% of Th present in the rock appear in the phosphoric acid itself, while 80% of Ra follows the so called phosphogypsum. This is an impure Ca sulfate that is removed as a precipitate during the process. Phosphogypsum is often discharged directly into estuaries, giving rise to a clear radioactive impact.

U, Th and Ra isotopes have been measured in water, suspended matter and sediment samples collected from the Odiel river (Periáñez & García-León, 1993; Periáñez et al., 1994b; Martínez-Aguirre et al., 1994a, b; Periáñez & Martínez-Aguirre, 1997a). These measurements have revealed a clear radioactive impact in the estuary due to the operation of the fertilizer complex. For instance, 670 mBq/l of ^{226}Ra, 131 mBq/l of ^{238}U and 5 mBq/l of ^{232}Th have been detected in waters collected close to the outlet of the complex. However, measurements

Fig. 2. Map of the Odiel estuary showing the sampling points (O1 to O7) and the fertilizer complex. The rectangular box is the grid used in the two dimensional model.

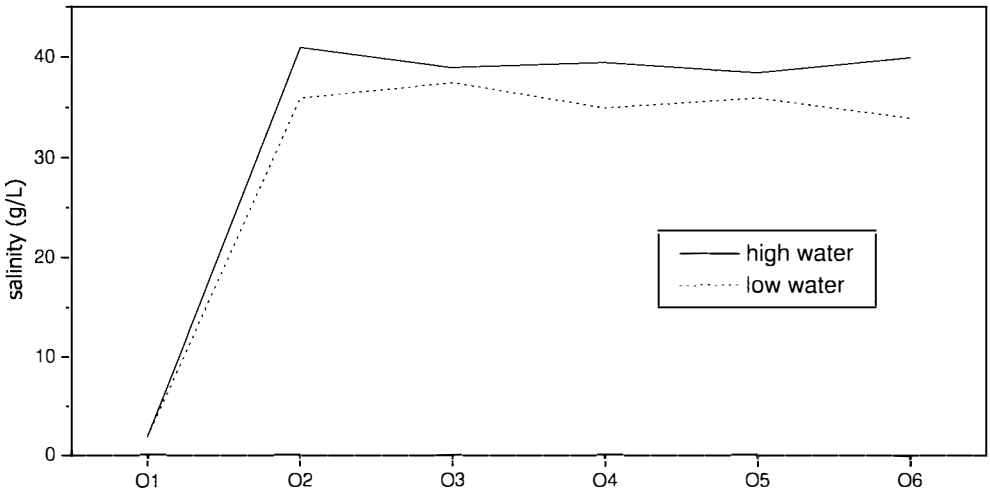

Fig. 3. Water salinity along the Odiel (g/l) for samples collected during high and low water.

have pointed out the complex behaviour and dynamics of radionuclides in the estuary. Indeed, water samples were collected during high and low water, and radionuclide concentrations were measured in water and suspended matter for both tidal states. A qualitative description of results is not an easy task since there is significant variability in activity concentrations and distribution coefficients, k_d, depending upon the sampling point and the tidal state. This is a logical result since we are dealing with an open system in which different effects are taking place at the same time: non constant input from the source, absorption–desorption reactions, deposition and erosion of the sediment, and water and suspended matter movements due to tides. Thus, the objective is to develop a model to describe the dispersion of these radionuclides in the estuary, including the distribution between the liquid and solid phases (suspended matter and bottom sediments) as well as the effect of tidal oscillations.

Two modelling approaches have been applied. First, the general dispersion patterns of radionuclides in the estuary have been studied. To do this, a 1D dispersion model for conservative radionuclides has been developed. The movement of contaminant patches, due to tidal oscillations, discharged in the estuary from the fertilizer complex can be followed with this model. However, this model can only be applied to radionuclides that remain in solution, and thus, can be used to give us a general idea of the way that advective dispersion takes place. Later, a detailed 2D depth averaged model as been developed to study the dispersion of non conservative radionuclides (including the interactions with the solid phases) in the area close to the fertilizer complex.

The 1D modelling approach is presented in the next section. Then, the 2D model is described.

2. General dispersion patterns for dissolved radionuclides: 1D approach

The 1D model has been developed for both the Odiel and Tinto rivers, since tide propagation can be considered as a one-dimensional phenomenon. The marsh area extending on the

right bank of the Odiel forms a complex multi-channeled system where little bathymetric or hydrodynamic data exists. Thus, its main connection to the Odiel river, the Canal del Burro (see map of Fig. 2), will be treated as an open boundary and recorded water elevations at this point will be used as boundary conditions. The end of the Juan Carlos I quay will be another open boundary, the upper tidal limits in the Odiel and Tinto rivers are the other two natural boundaries limiting our study area.

The objective of this 1D model consists of studying the basic features of the dispersion of dissolved radionuclides. One of its main aspects is the accurate calculation of hydraulic parameters at every possible water level. The model also runs under real tidal conditions: time series of recorded elevations, instead of simple harmonic constituents, are used for boundary conditions. The effects of atmospheric forcing and the longitudinal water surface gradients have also been included.

2.1. *1D-hydrodynamic and dispersion model for the Odiel and Tinto estuary: constitutive equations*

The model presented by Abril & Abdel-Aal (2000) and Abril et al. (2000), developed to study radionuclide dispersion in the Suez Canal, has been adapted to the estuary. Only the basic features will be presented here.

Let us consider a control volume in an open channel, defined by the reference cross-sectional area A and the differential length $\mathrm{d}x$ along the longitudinal x direction. The free surface is $\mathrm{d}S = B\,\mathrm{d}x$, B being the width of the channel at the cross-sectional area. The water elevation, z, measured from the bottom of the channel, varies with time and position along the channel (x). A, B and $\mathrm{d}S$ are functions of the location and of $z(x,t)$.

The continuity equation can be written as:

$$\mathrm{d}S\frac{\partial z}{\partial t} + \frac{\partial Q}{\partial x}\mathrm{d}x - Q_{\mathrm{T}} = 0, \tag{1}$$

where Q is the water flow through A (in m^3/s) and Q_{T} represents the flow from tributary waters at the position given by the spatial coordinate x.

A detailed treatment of the momentum equation can be found in Irving (1978). For our control volume, and considering the previous definitions, the equation is written as follows:

$$\frac{\partial Q(t)}{\partial t} + \frac{\partial}{\partial x}\left(\frac{Q^2}{A}\right) + Ag\frac{\partial}{\partial x}(z+N) = F_{\mathrm{fri}} - F_{\mathrm{win}}. \tag{2}$$

N is the elevation of the bed of the channel, referred to a fixed datum level, and its spatial derivative gives us the slope of the channel producing the gravitational forcing. Terms in the right side of the equation represent wind forcing, F_{win}, and friction, F_{fri}. The first has been adapted from Pugh (1987) and the second from French (1985).

As discussed in Abril & Abdel-Aal (2000), this mathematical formulation can be applied to channelled, shallow and well-mixed estuaries. Thus horizontal and vertical stratification is not considered.

The mass balance applied to a conservative tracer, with concentration $C(x,t)$, gives the following equation:

$$\frac{\partial C}{\partial t} + \frac{Q}{A}\frac{\partial C}{\partial x} = \frac{1}{A}\frac{\partial}{\partial x}\left(AD_x\frac{\partial C}{\partial x}\right) + \text{Sources}, \tag{3}$$

where a source and/or sink term is included. D_x is a diffusion coefficient parameterized as a function of the water velocity (shear effect) and the turbulent dispersion coefficient, D_{tur}:

$$D_x = D_{tur} + k_{sh}(Q/A)^2. \tag{4}$$

The hydrodynamic equations are solved using the numerical scheme presented in Prandle (1974). To avoid problems with numerical diffusion, a second order accuracy approximation to the upwind scheme has been applied to solve the advection term of equation (3). More specifically, a three-point formula, as presented in Kowalik & Murty (1993), has been used.

2.2. *1D-Hydrodynamics: input parameters and results*

To solve the equations, the studied area is divided in 53 sectors, each 1 km length. 31 sectors correspond to the Odiel, numbered upstream with sector 1 being the open boundary at the end of Juan Carlos I quay. The Tinto branch has 21 additional sectors, numbered consecutively from sector 16, the Odiel sector where the junction with the Tinto is located. Finally, 1 additional sector represents the entrance of the Canal del Burro, connecting with the Odiel at sector 17. Eight equispaced cross-sections are digitized, from marine and topographic charts, for each sector. A computer code was developed to produce the required hydraulic parameters as a function of the water elevation above or below each local mean sea level.

Tidal records are required to provide both the maximum tidal amplitude and appropriate boundary conditions. Tidal tables are available for sectors 5 and 21 in the Odiel (IHM, 1992). The Harbor Authority provided the tidal records and current measurements from a campaign contracted in 1989 with INTECSA. The data cover sectors 1, 5, 14 and C. Burro (elevations), and 5, 12, 14 and 18 (current magnitudes); all the sectors lie in the Odiel. These records correspond to some 24 hours of measurements carried out during three different tidal situations (spring, medium and neap tides). No information was available for the Tinto river. Thus, currents were measured at an intermediate sector during a complete tidal cycle (Laissaoui, 1999). This information is used for model calibration purposes.

Incoming water fluxes at the tidal limit of the Tinto and Odiel rivers were available from the Hydrographic Confederation of Guadiana. Wind velocity and direction is also known from the National Institute of Meteorology. The slope of the channel bed and the details for friction were unknown. Thus they are obtained from a trial and error exercise during the model calibration (Laissaoui, 1999).

Recorded water elevations at sector 1 (Odiel) and the Canal del Burro sector are used as boundary conditions.

The hydrodynamic module was run for a situation of medium tides. A comparison between computed and recorded tidal series is presented in Fig. 4. Measured and computed current amplitudes are presented in Fig. 5. Further calibration for the Tinto river was possible from the

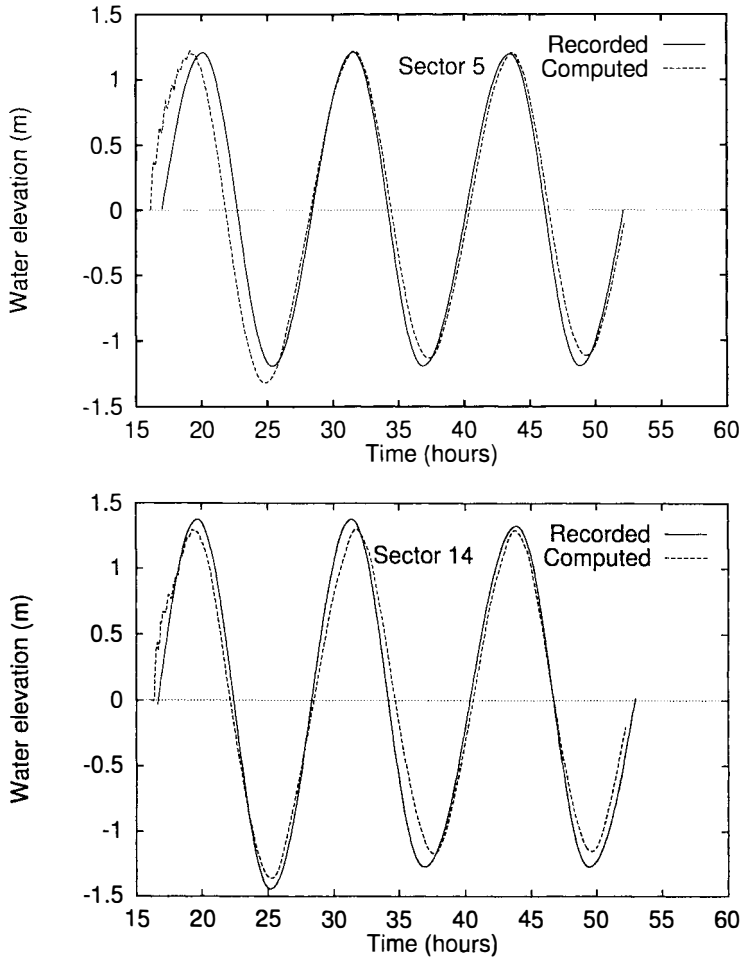

Fig. 4. Comparison between computed and recorded water elevations at several locations along the Odiel river in a situation of medium tides.

measured (for medium tide conditions) time series of velocities. Without any more changes, the hydrodynamic module was run for spring and neap tide conditions, producing reasonable agreement with the available data (Laissaoui, 1999). The model also showed its applicability under extreme conditions of spring tides and heavy rain.

2.3. *Computing the path for the centroid of a cloud of a conservative tracer*

Some numerical experiments have been carried out to study the fate of instantaneous discharges of any conservative pollutant released at Foret (a fertilizer plant placed at sector 20 in the Odiel river). The displacement of the centroid along the Odiel river has been evaluated from the computed instantaneous velocities at the location where the centroid is at each

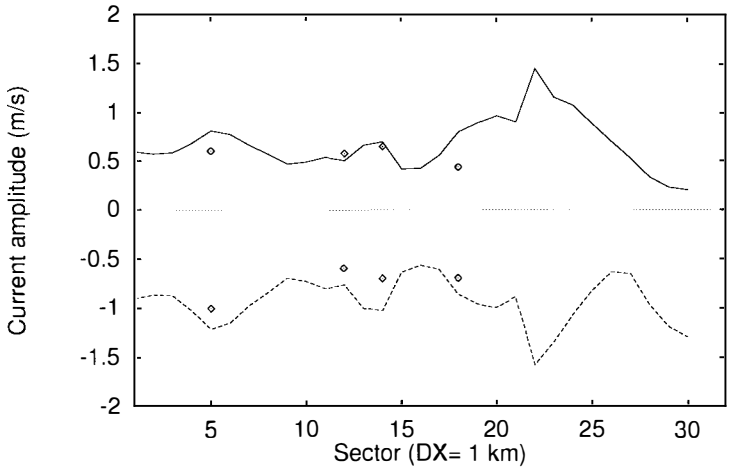

Fig. 5. Comparison between measured (points) and computed (lines) current amplitudes along the Odiel river (medium tides). Positive and negative values means upstream and downstream currents, respectively.

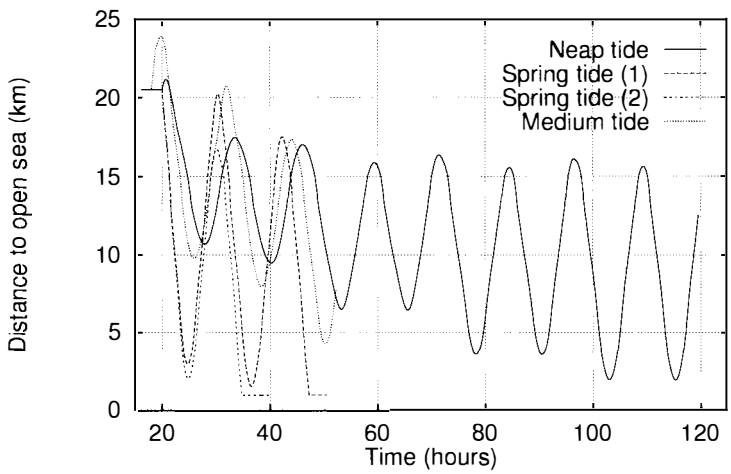

Fig. 6. Computed paths for an instantaneous release of a conservative tracer at Foret location. The figure shows the required time to reach sector 1 in the Odiel river as a function of different tidal and weather conditions (see text).

time step (eulerian transport, see Abril & Abdel-Aal, 2000). The aim is to evaluate the time required for the centroid to reach the open sea (crossing sector 1 in Odiel).

The position of the centroid versus the time after release, for different tidal and weather conditions, is shown in Fig. 6. The results correspond to medium, neap and spring tide situations, respectively, with river inputs of 3.1 (Odiel) and 107 m^3/s (Tinto). *Spring tide (2)* corresponds to spring tides and higher river inputs (1070 m^3/s at the Odiel, a typical value after heavy rain episodes). In all cases, the releases take place at the beginning of the ebb, which is the optimum situation for a faster cleaning of the system. It can be seen how for

medium tides the plume oscillates for several tidal cycles with some small downstream drift (the increase in oscillations is due to the neap-spring cycle). Oscillations are higher for spring tides, also with a higher drift current when a larger water flux comes from the upper river after heavy rain episodes. The plume leaves the estuary when the centroid reaches the zero level, although some contamination returns in the following high tide episode. From this, it can be concluded that *Juan Carlos I* quay (at the right bank of the Odiel river, from sectors 12 to 1) is hindering the natural cleaning of the waters. Thus, it is contributing to the production of higher levels of contamination within the estuarine area.

2.4. *1D-dispersion: some global aspects*

Some numerical experiments have been carried out with the dispersion model. Concentrations at the open boundaries are evaluated from an analytical fit to the tail of a Gaussian distribution, as in Abril & Abdel-Aal (2000). From our previous work in the southern Suez Canal (Abril et al., 2000), and from field tracing experiments in several Spanish rivers (Plata, 1985), k_{tur} in equation (4) has been fixed as 1 $m^2\ s^{-1}$, and a value of $k_{sh} = 5$ was adopted.

The model shows reasonable behaviour for the spatial and temporal evolution of the plume. For medium tide conditions, the tidal displacement of the centroid is some 10 km. Concentrations decrease roughly following a law of inverse proportionality to the square root of time (as expected from a Gaussian Model), but this law is broken at the Tinto and Burro connections. The plume can penetrate into the Tinto river only with the flood. It hardly reaches 10 km upstream, leaving this river with the ebb. Thus, concentrations in the Tinto river have to be related to those appearing downstream at the confluence of both rivers. During the ebb, a fraction of the pollutants extending over the upper Odiel river can leave the system through the Burro canal. Releases carried out during the flood can lead to a significant contamination of the upper marsh area of the Odiel river. In Fig. 7, an example of the temporal and spatial evolution of a conservative tracer plume is presented (situation of medium tides, initial plume of 1 km length with an homogeneous concentration of 1000 arbitrary units, located at sector 22 at the high water).

In a second modelling exercise we simulated the dispersion of a continuous discharge of ^{226}Ra, taking place at a constant rate of 1.1×10^4 Bq/s (a value suggested by Bolivar, 1995). The simulation extends over several days along a neap-spring-neap tidal cycle. At each sector, the time evolution of concentrations shows tidal oscillations over an asymptotic-like pattern of increase (see Fig. 8). The spatial maps of these concentrations give a picture of the estuary areas being more affected by the discharges. This is plotted in Fig. 9, during high water after 5 days. The distribution pattern shows the expected structure in which we can recognize higher concentrations around the source site in the Odiel, and a decreasing pattern from the junction to the upper tidal limit in the Tinto. Upstream from Foret, concentrations decrease due to the vicinity of the upper tidal limit and the fresh water inflow. A sensitivity test for boundary conditions is presented in Laissaoui (1999). As discussed in this reference, measured concentrations at different tidal and seasonal conditions show a similar pattern, but they are higher by a factor 4 in samples from the summer of 1990 (excluding a point sampled just at the pipe-line outlet). This factor is only 3 in samples from the spring of 1991, and is unity after the wash out effect of a week of heavy rains (also in samples from 1991). One possible explanation is that the real source term should be higher than that estimated by Bolivar (1995).

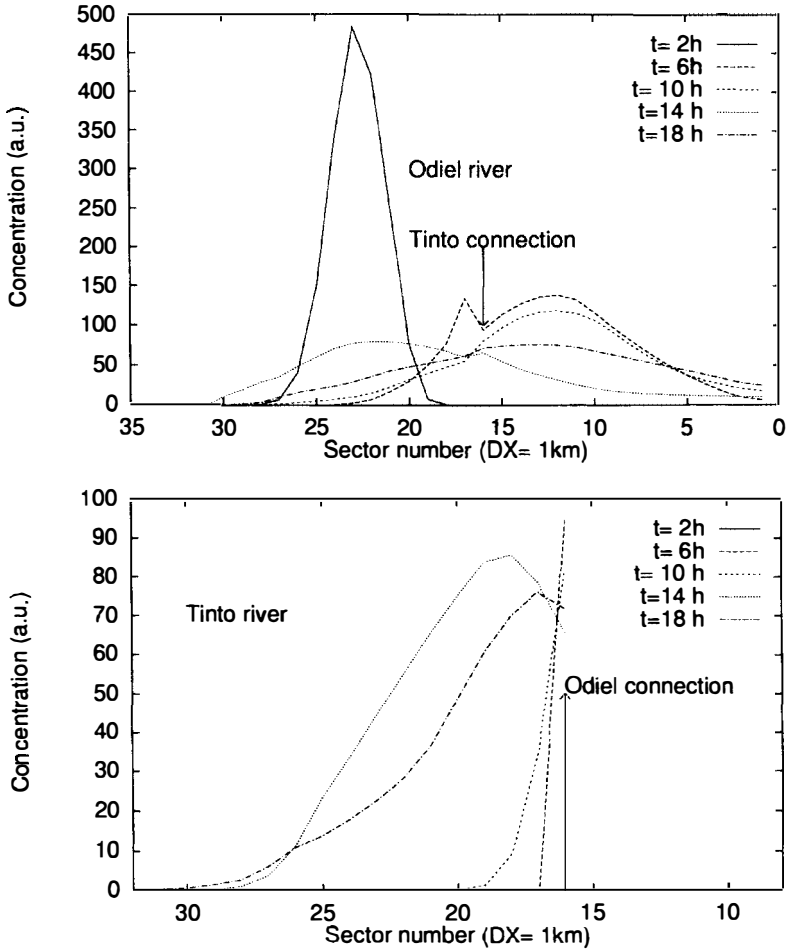

Fig. 7. An example of the spatial and temporal evolution of a conservative tracer plume in the Odiel an Tinto rivers (see text for an explanation of initial conditions and for the numbering of sectors). Concentrations are given in arbitrary units.

Also, non continuous discharges can add a more complex structure to the observed patterns. Finally, ^{226}Ra is not a totally conservative radionuclide. Thus, interactions with suspended matter and bottom sediments should be considered for a more realistic simulation.

3. A 2D model for non conservative radionuclides

The first models which were developed to simulate the dispersion of non conservative radionuclides in aquatic systems were averaged box models in which the exchanges between the liquid and solid phases were described in terms of equilibrium distribution coefficients k_d. However, in open systems and when studying dispersion in small coastal areas and estuaries

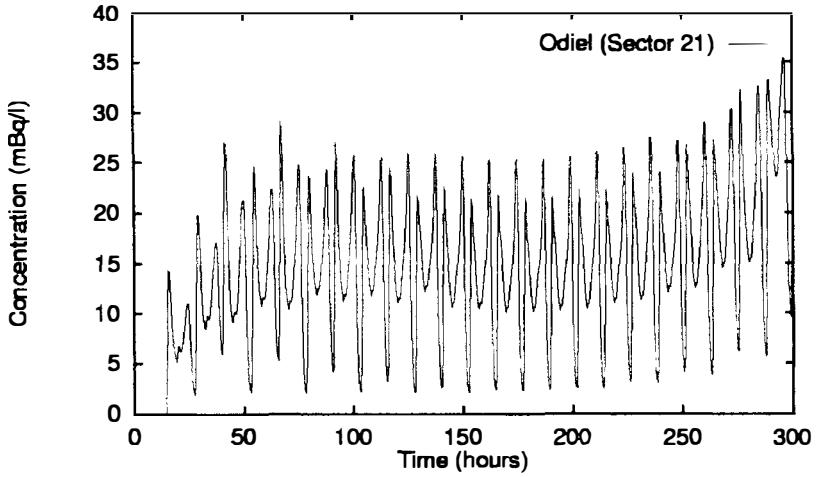

Fig. 8. Computed time evolution of ^{226}Ra concentration in sector 21 of the Odiel river. The simulation corresponds to a continuous discharge taking place at a constant rate and at Foret location (sector 20 in the Odiel).

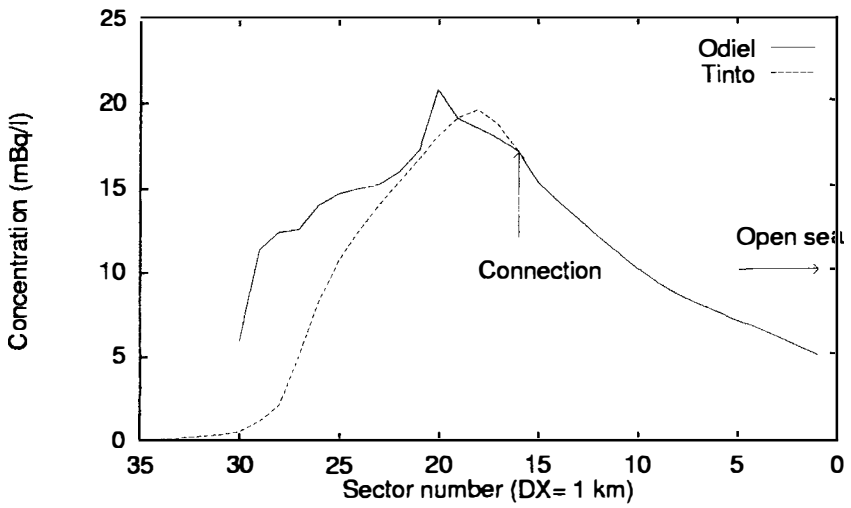

Fig. 9. Computed ^{226}Ra concentration obtained after 5 days of simulation during high water along the Odiel (solid line) and Tinto (dashed line) rivers for a continuous discharge at a constant rate.

the equilibrium approach will not hold due to the small time steps required in calculations: equilibrium will not be reached in each time step. In these cases a kinetic approach is more appropriate. Thus, the equilibrium will be the dynamic balance between two opposite chemical reactions (Nyffeler et al., 1984).

The system under study is divided into a number of grid cells. Four phases are present in each grid cell: water, suspended matter and two sediment grain size fractions. One grid cell is shown in Fig. 10. Radionuclides can be dissolved or associated with suspended matter. As

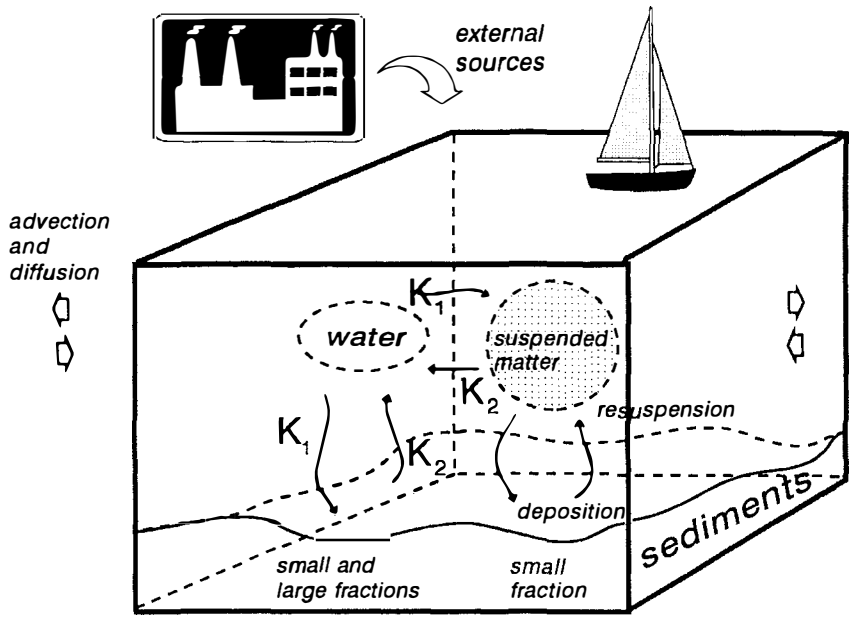

Fig. 10. Grid cell in which the radionuclide transfers between the four phases considered in the model are represented.

tides produce a continuous movement of water, radionuclides in these phases will be transported from one grid cell to another by advection and diffusion processes. Only particles with a diameter < 62.5 μm will be considered, as usual, to be present in the water column as suspended matter: larger particles will rapidly sink to the bottom and their horizontal movement is negligible. In sediments, two grain size fractions are considered, particles with a diameter < 62.5 μm (small grain size fraction) and particles with a diameter > 62.5 μm (large grain size fraction). Only the small grain size fraction particles can be resuspended and incorporated into the water column as suspended matter. On the other hand, when suspended matter particles are deposited on the bed sediment, they are incorporated into the small grain size sediment fraction. The dissolved phase is in contact with the other three phases, thus absorption-desorption reactions take place, which are described in terms of the kinetic transfer coefficients k_1 (transfer from water to the solid phases) and k_2 (desorption from the solid phases). Finally, external sources of radionuclides may exist in the grid cell.

It seems clear that the hydrodynamic and the suspended matter dynamic of the estuary must be solved to compute the advective transport of radionuclides and to obtain the suspended matter concentration and the erosion and deposition rates for each point of the estuary and for each instant of time.

3.1. *Hydrodynamics*

The 2D shallow water depth averaged hydrodynamic equations are (Pugh, 1987):

$$\frac{\partial z}{\partial t} + \frac{\partial}{\partial x}[(D+z)u] + \frac{\partial}{\partial y}[(D+z)v] = 0, \tag{5}$$

$$\frac{\partial u}{\partial t} + u\frac{\partial u}{\partial x} + v\frac{\partial u}{\partial y} + g\frac{\partial z}{\partial x} - \Omega v + K\frac{u\sqrt{u^2+v^2}}{D+z} = 0, \tag{6}$$

$$\frac{\partial v}{\partial t} + u\frac{\partial v}{\partial x} + v\frac{\partial v}{\partial y} + g\frac{\partial z}{\partial y} + \Omega u + K\frac{v\sqrt{u^2+v^2}}{D+z} = 0, \tag{7}$$

where u and v are the depth averaged water velocities along the x and y axis, D is the depth of water below the mean sea level, z is the displacement of the water surface above the mean sea level measured upwards, Ω is the Coriolis parameter ($\Omega = 2w\sin\beta$, where w is the earth rotational angular velocity and β is latitude), g is acceleration due to gravity and K is the bed friction coefficient. The effect of wind is included by adding the terms

$$-\frac{\rho_a}{\rho_w}\frac{C_D}{D+z}|W|W\cos\theta, \tag{8}$$

$$-\frac{\rho_a}{\rho_w}\frac{C_D}{D+z}|W|W\sin\theta \tag{9}$$

to the left-hand side of equations (6) and (7), respectively. ρ_a and ρ_w are the densities of air and water, W is the wind speed and θ is the direction to which wind blows measured anticlockwise from east. C_D is a drag coefficient. An acceptable value is (Pugh, 1987):

$$C_D = (0.63 + 0.066W) \times 10^{-3}, \tag{10}$$

if $2.5 < W < 21$ with W measured in m/s 10 m above the sea surface.

The part of the estuary that is covered by the 2D model is presented in Fig. 11, where water depths are also shown. A spatial discretization of the estuary is carried out to solve the equations by finite differences. Thus, the estuary is divided into a number of grid cells with sizes $\Delta x = \Delta y = 100$ m (see Fig. 11). The time step is fixed as $\Delta t = 6$ s. In this way the CFL (Kowalick & Murty, 1993) condition is satisfied. In particular, the explicit finite difference scheme described in Flather & Heaps (1975) has been applied. Water elevations were specified along the southern open boundary of the computational domain and a radiation condition was applied at the northern boundary. The bed friction coefficient was fixed at $K = 0.0025$ after a calibration process. The output of the model has been compared with observations in situations of medium and neap tides. This is presented in detail in Periáñez et al. (1994a). As an example, a corange chart for the M_2 tide is presented in Fig. 12, where it can be seen that the amplitude of the tide increases as it goes inwards along the estuary. The time evolution, over several tidal cycles, of water elevations and currents at a point close to the southern boundary of the grid is shown in Fig. 13. It can be seen that currents in the transverse direction of the estuary (u component) are weaker than currents in the longitudinal direction (v component), so that the water movement is essentially directed along the axis of the estuary.

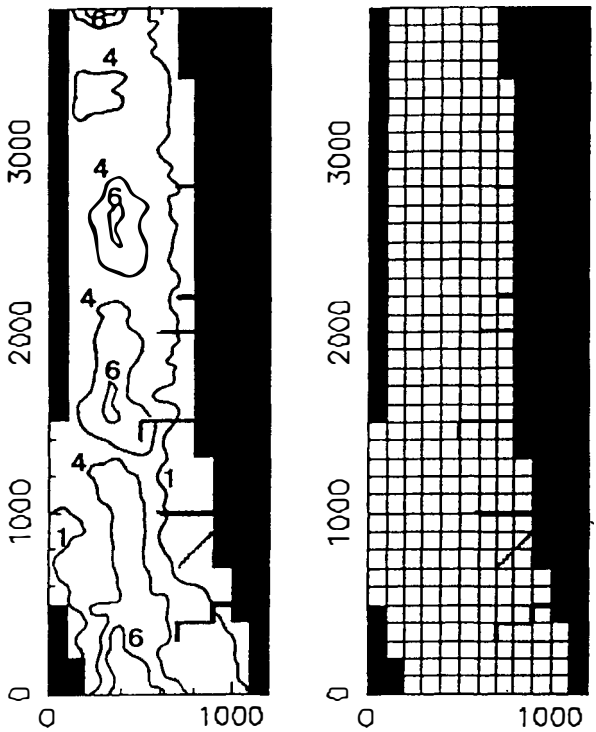

Fig. 11. Map of the part of the estuary covered by the 2D model (depths are given in m). The grid used for computations is also shown. Each unit in the x and y axis is 1 m.

3.2. *Suspended matter dynamics*

It is assumed that each grid cell contains a certain amount of suspended matter, m, in g/m^3 with an homogeneous distribution in the water column. This is realistic since, as commented above, the estuary is shallow and mixing between fresh and salt water takes place upstream of the modelled area. Also, the flow of the river is low and a fast dispersion of fresh water into a much larger volume of salt water occurs (Borrego & Pendon, 1988), as usual in tidal estuaries of small rivers (Eisma, 1993).

As usual in suspended matter studies, we will consider that only particles with a diameter < 62.5 μm can remain in the water column as suspended matter (Belderson, 1964; Clarke, 1995). Indeed, Eisma (1981) has pointed out that for all practical purposes, muds can be regarded as synonymous with suspended matter. The suspended matter equation is (Periáñez et al., 1996a):

$$\frac{\partial(Hm)}{\partial t} + \frac{\partial(uHm)}{\partial x} + \frac{\partial(vHm)}{\partial y} = \frac{\partial}{\partial x}\left(HK_x\frac{\partial m}{\partial x}\right) + \frac{\partial}{\partial y}\left(HK_y\frac{\partial m}{\partial y}\right)$$
$$- w_s m\left(1 - \frac{q}{q_{cd}}\right) + v_r\rho_s f 10^3\left(\frac{q}{q_{cc}} - 1\right), \qquad (11)$$

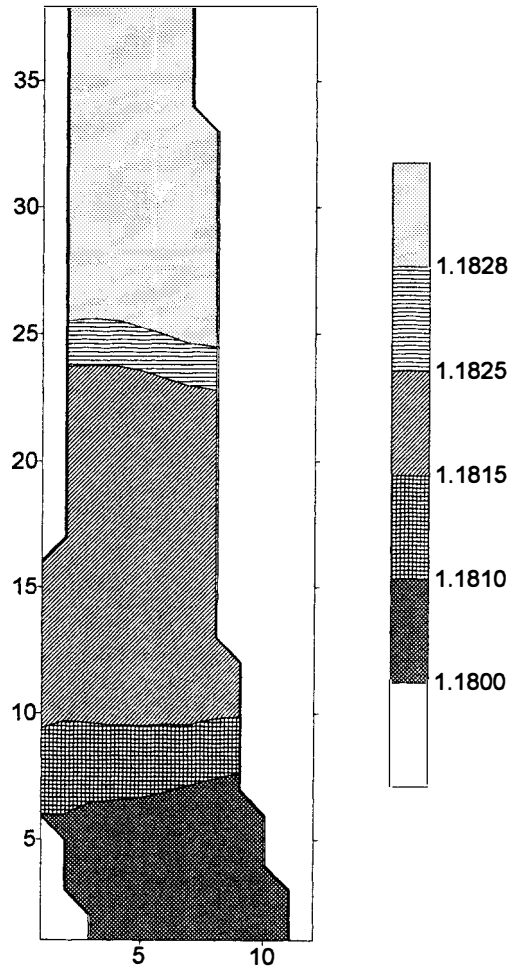

Fig. 12. Computed corange chart for the M_2 tide. Tidal amplitudes are given in m. x and y axis denote the grid cell number, thus each unit corresponds to 100 m.

where $H = D + z$ is the total water depth, and K_x and K_y are the diffusion coefficients in the x and y directions, respectively. The last two terms represent deposition and erosion: w_s is the settling velocity of suspended particles, $q = \overline{\sqrt{u^2 + v^2}}$ is the current magnitude, v_r is a resuspension velocity from the sediment, ρ_s is the dry matter density of the sediment (in kg/m^3) and f gives the fraction of small particles in the sediment. q_{cd} and q_{ce} are threshold currents for deposition and erosion, respectively. Thus, it is considered that deposition of particles can occur only if the current is smaller than q_{cd}. Similarly, there is erosion of the sediment only if the current is larger than a critical value q_{ce}. If any of these conditions is not satisfied, the corresponding term is set to zero.

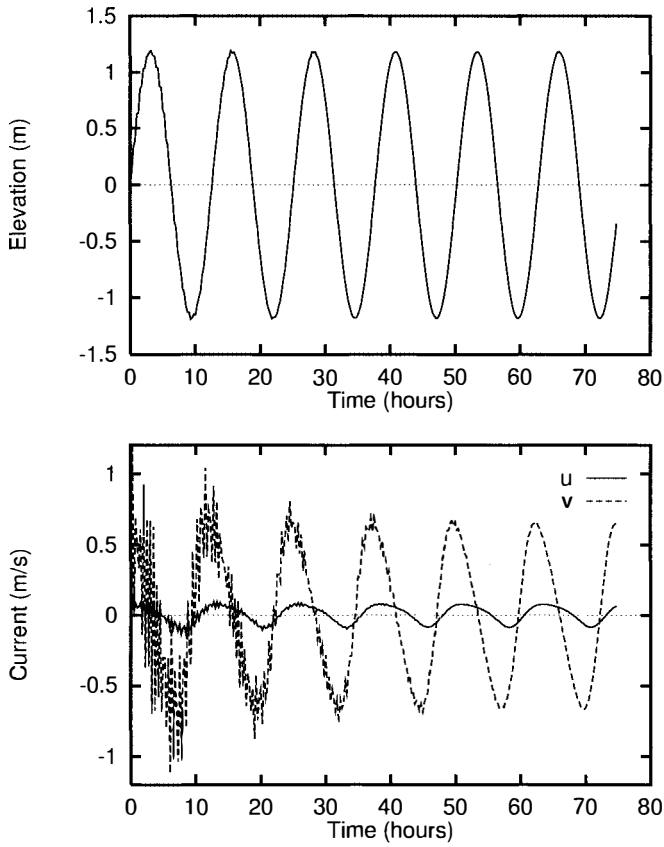

Fig. 13. Time evolution of computed water elevations (m) and components u and v of the current (m/s) in a point located close to the southern boundary of the grid for the M_2 tide.

The description of Prandle (1984) was used for the diffusion coefficients:

$$K_x = \beta_1 |u| q, \tag{12}$$

$$K_y = \beta_2 |v| q, \tag{13}$$

where β_1 and β_2 are numeric factors to be calibrated for each specific site.

The settling velocity of suspended particles increases, at low concentrations (smaller than 1000 ppm), as the suspended matter concentration increases due to flocculation of particles. A standard formula to represent this process is (Pejrup, 1988; Mehta, 1989; Clarke, 1995):

$$w_s = a_1 m^{a_2}, \tag{14}$$

where a_1 and a_2 have to be obtained from observations or from model calibration.

The solution of the suspended matter equation provides the suspended matter concentration at each position of the grid and at each instant of time.

In the case of the Odiel river, $\beta_1 = \beta_2 = 1000$ s (Periáñez et al., 1994a, 1996a); $a_1 = 1.74 \times 10^{-9}$ and $a_2 = 1.6$, which are the values found by Mehta (1989); $q_{cd} = 0.18$ m/s (Eisma, 1993) and $v_r = 9.6 \times 10^{-7}$ m/s (Periáñez et al., 1996a). The erosion threshold velocity depends on the roughness length of the sediment, z_0. From data in Pugh (1987), an analytical function relating q_{ce} and z_0 has been constructed:

$$q_{ce} = 0.441 e^{-1.117 z_0^{0.231}}, \tag{15}$$

if q_{ce} is expressed in m/s and z_0 in cm. Values of f, ρ_s and z_0 over the estuary have been obtained from measurements (Universidad de Sevilla, 1991).

The suspended matter equation has also been solved using finite differences. The first order upwind scheme was used for the advective terms and a second order explicit scheme for the diffusion ones. Both are presented in Kowalick & Murty (1993). It is known that the upwind scheme introduces numerical diffusion. However, it has been proved (Periáñez et al., 1994a) that this is negligible in the present model due to the small size of the grid cells.

The boundary condition in the northern boundary of the grid consists of making the suspended matter concentration in the last row equal to that of the previous row. Along the southern boundary, suspended matter concentrations were specified for each time step from observations: a sampling campaign was performed so that water samples were collected every 20 min during a complete tidal cycle in both the southern and northern borders of the grid. Suspended matter concentrations were measured using a calibrated nephelometer (Periáñez, 1995); results can be seen in Fig. 14.

The time evolution of computed suspended matter concentrations in three grid cells can be seen in Fig. 15. As we move towards the north of the grid, oscillations in suspended matter decrease. Indeed, the suspended matter concentration in the cell near the northern border is almost constant. This behaviour has been observed in the Odiel estuary: Fig. 14 shows that concentrations at the northern border are quite constant, with a mean value 28 ± 4 ppm. The computed mean value is 24.4 ppm, in good agreement with observations. This behaviour is due to the fact that water velocities decrease as we move towards the north (Periáñez et al., 1994a), so resuspension becomes negligible and deposition must be essentially constant along the tidal cycle. Thus, oscillations in suspended matter concentrations vanish. On the other hand, it can be seen in Fig. 15 that there are two peaks in concentrations for each tidal cycle in the south of the grid: during flood and ebb. In these situations currents are stronger and erosion of the sediment occurs. During high and low water, deposition takes place and the suspended load reaches a minimum. A double peak in m is due to the combination of the quarterly diurnal signal of resuspended material with the semi diurnal signal of advected material (Williams et al., 1998).

Suspended matter concentration maps, when water level is increasing and decreasing, can be seen in Fig. 16. The decrease in concentrations as we move towards the north can be clearly seen here.

Also, the model can give information about the net sedimentation rates in the estuary (see Periáñez et al., 1996a for details).

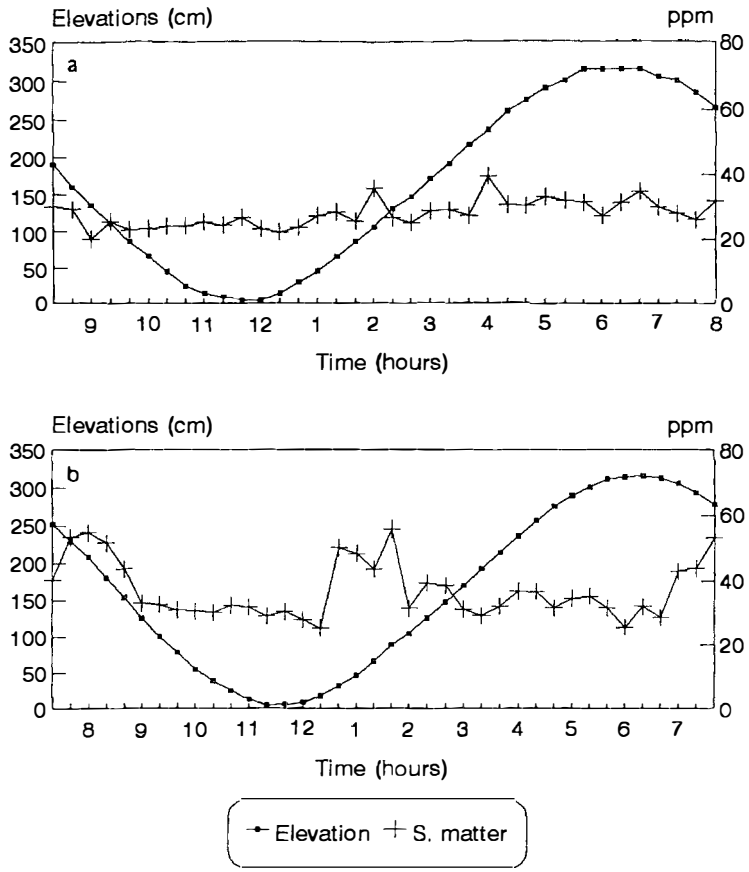

Fig. 14. Suspended matter concentrations (ppm) measured in the northern (a) and southern (b) boundaries of the grid over a tidal cycle. Water elevations are given with respect an arbitrary reference.

3.3. *Radionuclide equations*

As commented above, transfers of radionuclides between the liquid and solid phases will be described in terms of kinetic transfer coefficients. A coefficient k_1 governs the transfer from water to the solid phases and a coefficient k_2 governs the inverse process.

The absorption process is a surface phenomenon that will depend on the surface of particles per water volume unit into the grid cell. This quantity is denoted as the exchange surface (Periáñez et al., 1996b). Thus, the kinetic transfer coefficient k_1 will be proportional to the exchange surface:

$$k_1 = \chi_1 (S_m + S_s + S_l), \tag{16}$$

where the proportionality factor χ_1 has the dimensions of a velocity and is denoted as the exchange velocity (Periáñez et al., 1996b). It is related to the molecular velocity of dissolved radionuclides, which at the same time is related to the temperature of water. S_m, S_s and S_l are,

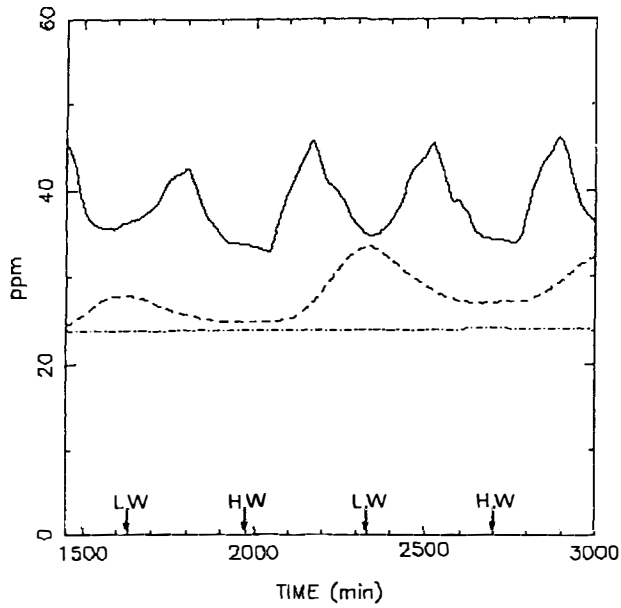

Fig. 15. Time evolution of the suspended matter concentration in three grid cells: near the southern border (solid line), in the middle of the grid (dashed line) and near the northern border (dashed dotted line). The moments at which high and low water occur are also shown.

respectively, the exchange surfaces for suspended matter, the small and the large grain size fractions of sediments.

As a first approach, assuming spherical particles and a step function for the grain size distribution of particles, it can be easily shown (Periáñez et al., 1996b) that:

$$S_{\mathrm{m}} = \frac{3m}{\rho R}, \tag{17}$$

where ρ and R are density and mean radius of suspended matter particles, respectively.

The water-sediment interface can be considered as a high suspended matter environment (Li et al., 1984). Thus, the exchange surfaces for both sediment fractions are (Periáñez et al., 1996b):

$$S_{\mathrm{s}} = \frac{3Lf\phi}{RH}, \tag{18}$$

$$S_{\mathrm{l}} = \frac{3L(1-f)\phi'}{R_{\mathrm{l}}H}, \tag{19}$$

where L is the average mixing depth (the distance to which the dissolved phase penetrates the sediment), R_{l} is the mean radius of particles of the large grain size sediment fraction and ϕ and ϕ' are correction factors that take into account that not all the surface of the sediment

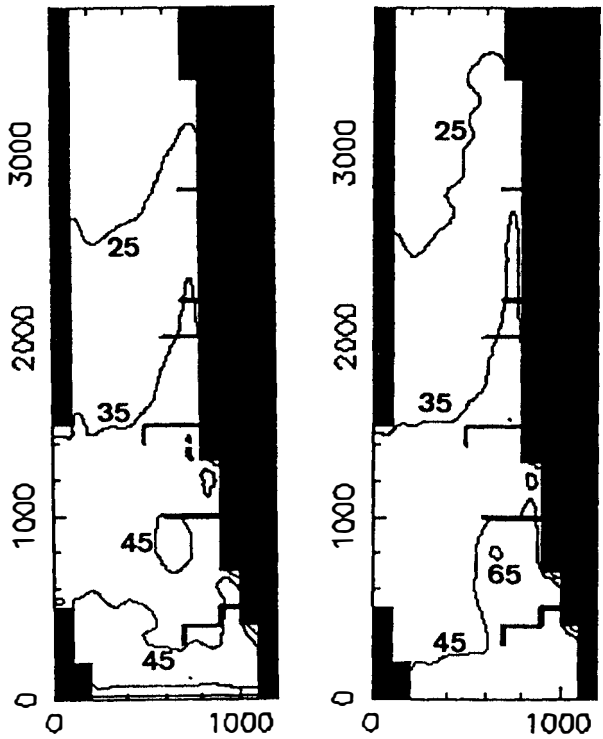

Fig. 16. Suspended matter concentration (ppm) maps when water level is increasing (a) and decreasing (b). Each unit in the x and y axis is 1 m.

particle is in contact with water, since it will be partially hidden by other particles. Thus, the total k_1 coefficient can be written as:

$$k_1 = \chi_1 \left(\frac{3m}{\rho R} + \frac{3Lf\phi}{RH} + \frac{3L(1-f)\phi'}{R_1 H} \right). \tag{20}$$

It is interesting to note that k_1 is proportional to the suspended matter concentration. Indeed, some laboratory experiments (Benes et al., 1992; Benes & Cernik, 1992) have shown that a direct relation between both exists. Equation (20) is the analytical form of such a relation.

The equation that gives the time evolution of specific activity in the dissolved phase, C_d (Bq/m^3), is:

$$\frac{\partial(C_d H)}{\partial t} = (\text{adv} + \text{dif}) - k_1 C_d H + k_2 C_s m H + k_2 L \rho_s 10^3 \left[f\phi A_s + (1-f)\phi' A_1 \right], \tag{21}$$

where (adv + dif) means advective plus diffusive transport of radionuclides, C_s (Bq/g), A_s (Bq/g) and A_1 (Bq/g) are, respectively, specific activities in suspended matter, small and large

grain size fractions of sediments. The external source of radionuclides should be added to this equation at the points where it exists. The transfer coefficient k_1 is given by equation (20).

The equation for the time evolution of specific activity in suspended matter particles is:

$$\frac{\partial(mC_sH)}{\partial t} = (\text{adv} + \text{dif}) + k_1 C_d H - k_2 m C_s H + (\text{er} - \text{dep}), \tag{22}$$

where k_1 is given by the first term of equation (20) and the deposition and erosion terms are given by:

$$\text{dep} = w_s m C_s \left(1 - \frac{q}{q_{cd}}\right), \tag{23}$$

$$\text{er} = v_r \rho_s f A_s 10^3 \left(\frac{q}{q_{ce}} - 1\right). \tag{24}$$

Again, a source term should be included in this equation if an external input of radionuclides fixed to solid particles exists.

The small grain size fraction of the sediment exchanges radionuclides with the dissolved phase and with suspended matter, through erosion and deposition. The corresponding equation is:

$$\frac{\partial A_s}{\partial t} = k_1 \frac{C_d H}{L \rho_s f} 10^{-3} - k_2 A_s \phi + (\text{dep} - \text{er}), \tag{25}$$

where k_1 is given by the second term in equation (20) and the erosion and deposition terms are:

$$\text{er} = \frac{v_r A_s}{L}\left(\frac{q}{q_{ce}} - 1\right), \tag{26}$$

$$\text{dep} = \frac{w_s m C_s}{L \rho_s f} 10^{-3}\left(1 - \frac{q}{q_{cd}}\right). \tag{27}$$

Finally, the large grain size fraction of the sediment exchanges radionuclides only with the dissolved phase:

$$\frac{\partial A_l}{\partial t} = k_1 \frac{C_d H}{L \rho_s (1 - f)} 10^{-3} - k_2 A_l \phi', \tag{28}$$

where k_1 is now given by the third term in equation (20). Specific activity in the total sediment will be:

$$A_{\text{total}} = f A_s + (1 - f) A_l. \tag{29}$$

This description of the dispersion of non conservative radionuclides has been applied to simulate the transport of ^{226}Ra, ^{238}U and ^{232}Th in the Odiel estuary, as will be shown below.

However, it has been applied to other environments to show the universality of the description. Thus, it has been applied to simulate the dispersion of ^{137}Cs and ^{239,240}Pu in the English Channel (Periáñez, 2000a) and to simulate the dispersion of ^{239,240}Pu in the eastern Irish Sea (Periáñez, 1999, 2000b). In this latter case, the formulation has been extended to a three dimensional description. A very similar description has also been used by other authors to simulate the dispersion of radionuclides in the sea (Aldridge, 1998; Margvelashvily et al., 1997).

3.4. *k_d description*

Suspended matter–water distribution coefficients are experimentally obtained as the specific activity in suspended matter divided by the specific activity in water. Absorption–desorption reactions take place only over the surface layer of suspended particles. The central part of particles cannot interact with the liquid phase. Specific activity in suspended matter, C_s, that is calculated by equation (22), refers to specific activity in this surface layer, that is the activity in the surface layer of suspended matter particles divided by the total mass of suspended particles. However, we are interested in modelling Ra, U and Th dispersion, which are natural radionuclides and thus, will also be present in the central part of particles. These radionuclides are considered when an experimental determination of k_d is carried out. They will be included in the model by assuming that there is a constant specific activity, for each radionuclide, in the central part of particles (supposed to be constant since radionuclides are locked in particles). C_s is then corrected adding to its value, such specific activity in the central part of particles. This specific activity is estimated from field information. The corrected radionuclide concentration in suspended matter is used to compute k_d values and is the presented concentration when results corresponding to specific activity in suspended matter are shown.

3.5. *Dispersion of ^{226}Ra, ^{238}U and ^{232}Th in the Odiel estuary*

3.5.1. *Parameters for the model*

The different parameters involved in the description of the dispersion of radionuclides have to be obtained from field measurements or from model calibration.

The density of particles in suspension has been taken as $\rho = 2600$ kg/m^3, which is the established value for the density of soil particles (Baver et al., 1992). As commented above, it is considered that suspended matter and the small grain size fraction of the sediment are composed of particles with a diameter < 62.5 μm. Thus, the mean radius of such particles is fixed as $R = 15$ μm. The mean radius of the large grain size fraction has been estimated (Periáñez et al., 1996c) from measurements (Universidad de Sevilla, 1991): $R_l = 440$ μm. After a calibration exercise, the mixing depth and the correction factors for the sediments were selected as $L = 0.1$ m, $\phi = 0.01$ and $\phi' = 0.005$. Some sensitivity tests to study the model response to changes in these parameters can be seen in Periáñez et al. (1996c).

In the case of ^{226}Ra, the coefficients χ_1 and k_2, which govern the transfers between the dissolved and solid phases, were obtained from laboratory experiments (Laissaoui et al., 1998). They consist of tracing, at the laboratory, unfiltered Odiel estuary water with a ^{133}Ba solution, a γ emitter whose chemical behaviour is similar to that of Ra. Conditions at the laboratory were as close as possible to natural conditions (temperature, pH, movement of water). The

time increase of the ^{133}Ba activity in suspended matter allows the calculation of both coefficients from a numerical fitting to the analytical solution of the corresponding differential equations. Details can be seen in the above mentioned reference. Results are: $\chi_1 = 0.55 \times 10^{-7}$ m/s and $k_2 = 8.17 \times 10^{-6}$ s^{-1}. Nevertheless, these coefficients may change slightly from one season to another due to changes in water conditions (salinity and temperature). Thus, some sensitivity tests to study the model response to these changes are presented in Periáñez et al. (1996c).

In previous work (Nyffeler et al., 1984), kinetic transfer coefficients were measured for a wide set of elements. It was found that there was very small variation in k_2 (less than an order of magnitude) for elements with very different geochemical behaviour (Th, Hg, Pa, Zn, Sb, Cs, Se, Cd, Ba, Sr, Na). This small variation opens the possibility, as suggested by Nyffeler et al. (1984), of estimating χ_1 without laboratory experiments. Indeed, it has been shown (Periáñez et al., 1996c) that the following relation between χ_1, k_2 and the suspended matter–water distribution coefficient, k_d, holds:

$$k_d = \frac{\chi_1}{k_2} \frac{3}{\rho R}. \tag{30}$$

Thus, the χ_1 values for U and Th can be obtained from the k_2 of Ba (obtained from the laboratory experiments carried out with Odiel waters) and the corresponding k_d of U and Th measured in the estuary. The mean value of the U distribution coefficient in the estuary is in agreement with the value presented in IAEA (1985) (see Periáñez & Martínez-Aguirre, 1997a): 1 l/g. In the case of Th, measured k_ds are lower than the average value given in IAEA (1985). The mean k_d value in the estuary, for Th, is 13.7 l/g (Periáñez & Martínez-Aguirre, 1997a). From equation (30) and the corresponding k_d values, it is finally obtained that for U, $\chi_1 = 1.06 \times 10^{-7}$ m/s, and for Th the exchange velocity is $\chi_1 = 1.46 \times 10^{-6}$ m/s. The exchange velocity of Th is an order of magnitude larger than that of U, revealing a larger affinity of Th to be fixed to the solid phases. These exchange velocities, although not exact values, seem to be good estimates since the model produces, as will be seen, results that are, in general, in agreement with experimental data.

3.5.2. *Results*

As the rate of change of activity in the sediment is slow, there are no significant changes during the typical simulated times (some days). Consequently, we use experimental values of specific activities in the sediments as initial conditions. These have been taken from Martínez-Aguirre et al. (1994a).

Samples in the Odiel estuary were collected, as commented above, during high and low water, with a time difference of 18 hours between them (19th and 20th July, 1990). Generally speaking, activity peaks should correspond with discharges performed shortly before or during sampling, while, when a flat distribution is measured, it should correspond with the background that remains in the river after the earlier homogenization of discharges. Activities released to the estuary from the fertilizer complex are not known. Thus, the magnitudes of the activity inputs were changed, by trial and error, until model output was in agreement with observations.

Thus, to reproduce the sampling conditions a first activity input was introduced in tidal cycle 1 and lasted 3.3 h. High water concentrations were obtained 2 cycles later (cycle 3).

A second activity input started in cycle 4 and lasted 9 h. Low water concentrations were obtained from this cycle. In this way, 18 h elapsed between the time-points in which concentrations for high and low water are obtained. The initial conditions applied to the dispersion model consisted of making $C_d = C_s = 0$ over the grid. However, in the Odiel estuary a significant background activity exists. In the case of ^{226}Ra, the first activity inputs were 9.0×10^7 and 9.9×10^6 Bq per time step for the dissolved phase and the suspended matter, respectively. During the second input, they were, respectively, 2.0×10^4 and 2.5×10^3 Bq per time step. Thus, the first input is larger than the second because it is used to create such a background, and 2 cycles are allowed to elapse so as to distribute the released radionuclides along the estuary. It has been shown (Periáñez et al., 1994a) that this method of creating the background does not influence the results.

Wind speed and direction corresponding to the date of sampling were used in the model (Periáñez et al., 1994a).

As can be seen in Fig. 17, there is a good agreement between observed and computed specific activities in both phases (water and suspended matter) and for both tidal states. Computed concentrations correspond to longitudinal sections of the estuary following the points where samples were collected. Sediments are not included in the discussion because there are no apparent changes in their specific activities during a time period of the order of some days. k_d distribution coefficients between suspended matter and water have also been calculated with the model, and are presented in Fig. 18 for high and low water together with their observed values. The general behaviour of distribution coefficients along the estuary is reproduced by the model.

The time sequence of activity inputs in the cases of ^{238}U and ^{232}Th is the same as that of ^{226}Ra, since specific activities for these radionuclides were obtained from the same set of samples. In the case of U, the first inputs were 1.4×10^6 and 1.1×10^2 mg of U per time step for the dissolved phase and suspended matter, respectively. For the second input, the corresponding rates were 1.3×10^6 and 1.0×10^2 mg per time step. It can be seen in Fig. 19 that there is a good agreement between computed and observed concentrations of U in both phases (however, dissolved U in high water could not be measured and thus, the model output could not be compared with observations in this case). Measured and computed distribution coefficients for the low water samples are presented in Fig. 20. The model reproduces the general behaviour of the k_d along the estuary.

In the case of Th, the first input rates were 3.3×10^4 and 2.6×10^2 mg per time step for the dissolved phase and suspended matter respectively. Rates were, respectively, 1.9×10^4 and 1.5×10^2 mg per time step for the second input.

Experimental and model results are presented in Fig. 21. The general behaviour of Th is well reproduced by the model. It is interesting to note that the model is able to reproduce spatial variations in concentrations of three orders of magnitude. As in the case of U, results for the dissolved phase in the high water samples could not be compared with observations. Computed and measured k_d for the low water samples are shown in Fig. 22.

The Th/U mass ratios have also been investigated with the model. They are presented in Fig. 23. An excess of U with respect to Th in suspended matter reveals an external source of U contaminated particles to the estuary (Periáñez & Martínez-Aguirre, 1997a; Periáñez et al., 1996d). However, close to the fertilizer complex there is an excess of Th with respect to U, which corresponds to the most contaminated area. Indeed more Th than U has been discharged

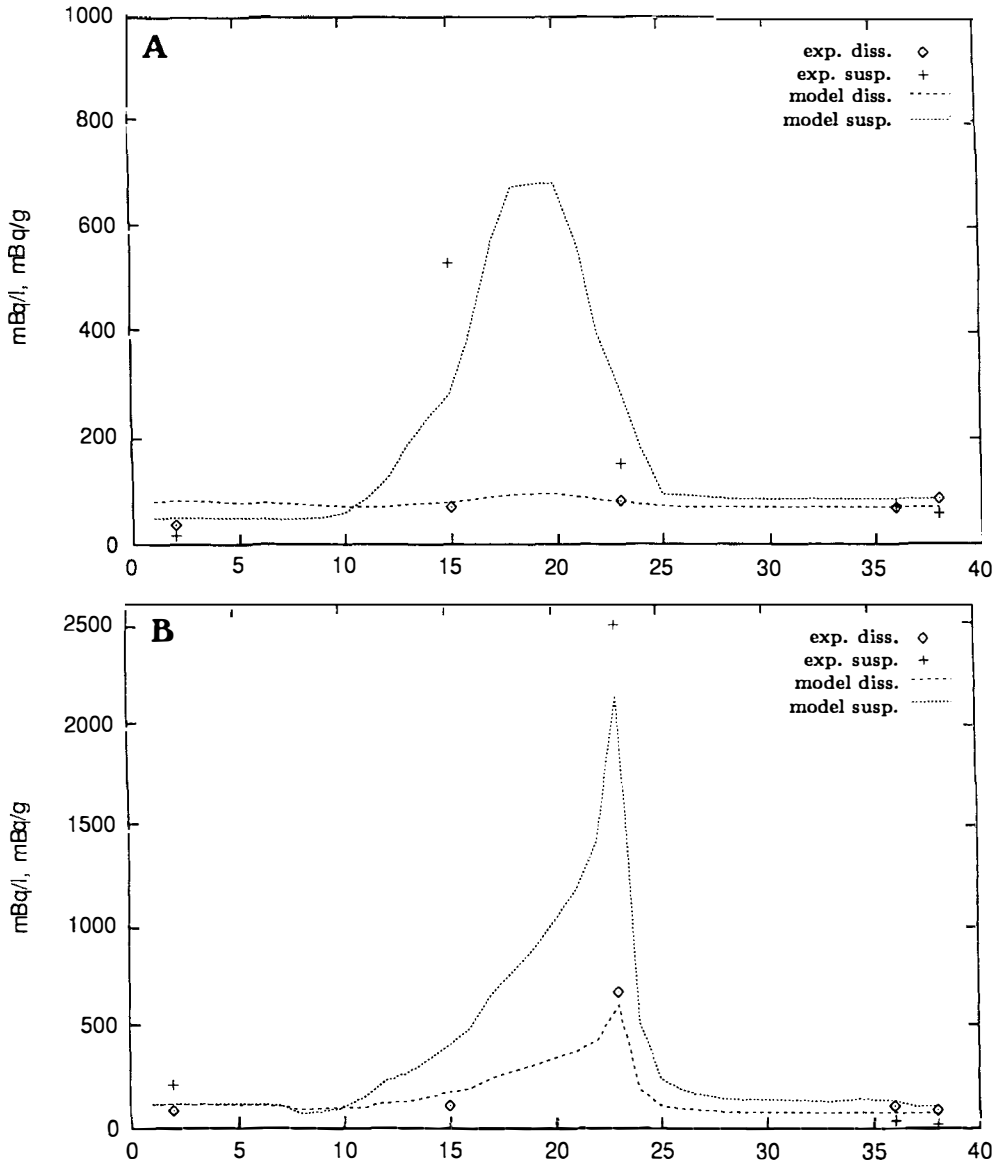

Fig. 17. Model results for high (A) and low (B) water samples. ^{226}Ra concentrations in water are given in mBq/l and in suspended matter in mBq/g. Points correspond to the measured concentrations are lines are the model results. The x axis is the position in the grid (grid cell number), thus each unit corresponds to 100 m.

to the estuary. From the second input rates (to obtain low water levels) Th/U = 2.4 in solution and Th/U = 1.5 in suspended matter. As a consequence, there is an excess of Th in both phases close to the source. In contrast, there is an excess of U in the rest of the estuary and in both phases. It seems that the dissolved Th that is released to the estuary is quickly fixed to

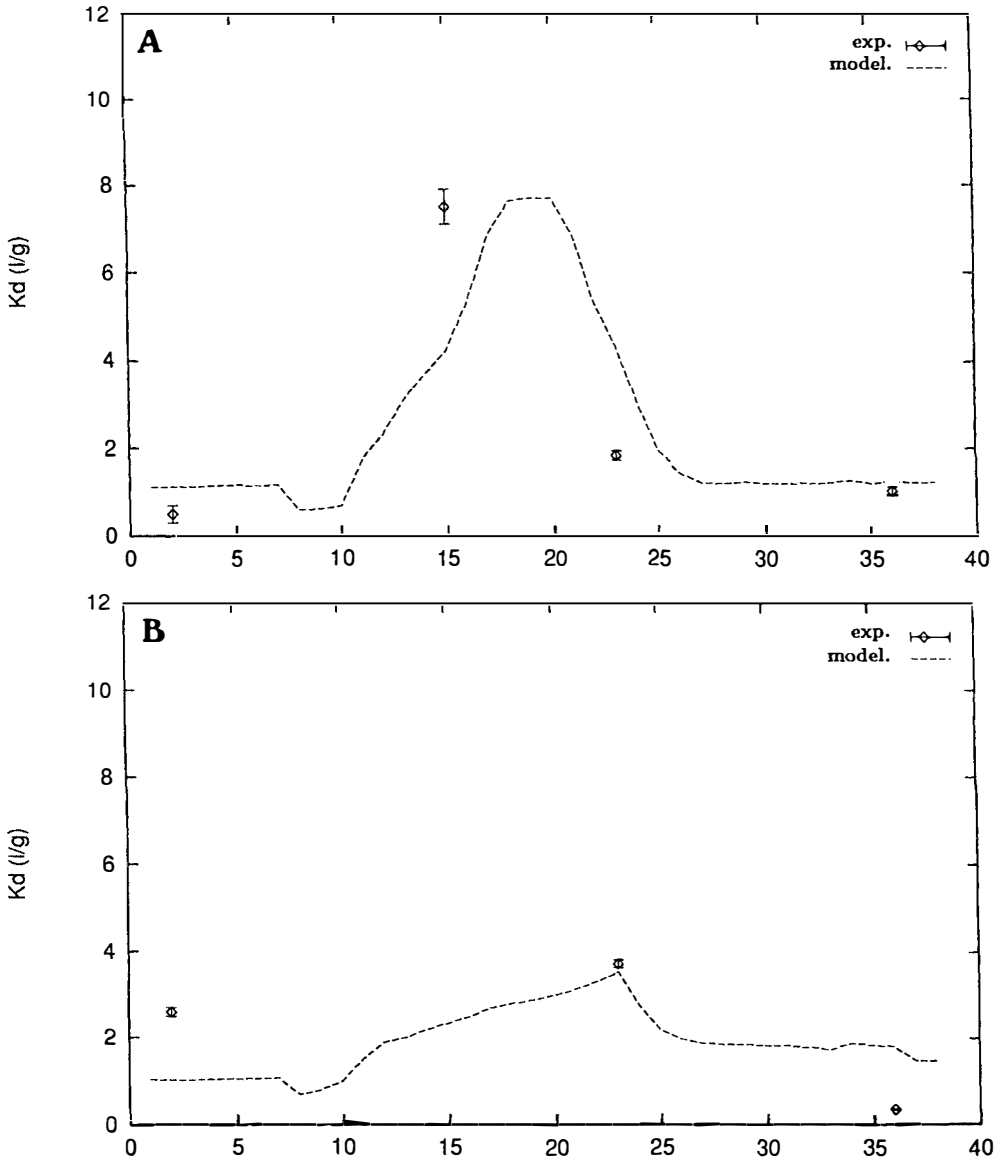

Fig. 18. Computed and measured ^{226}Ra distribution coefficients (l/g) for the high (A) and low (B) water samples.

the solid phase (bottom sediments and suspended matter particles). These particles, together with Th contaminated particles released from the source, are deposited on the estuary bed near the fertilizer complex. This could explain the U excess that is obtained in the rest of the estuary from both measurements and computations. This hypothesis is also supported by

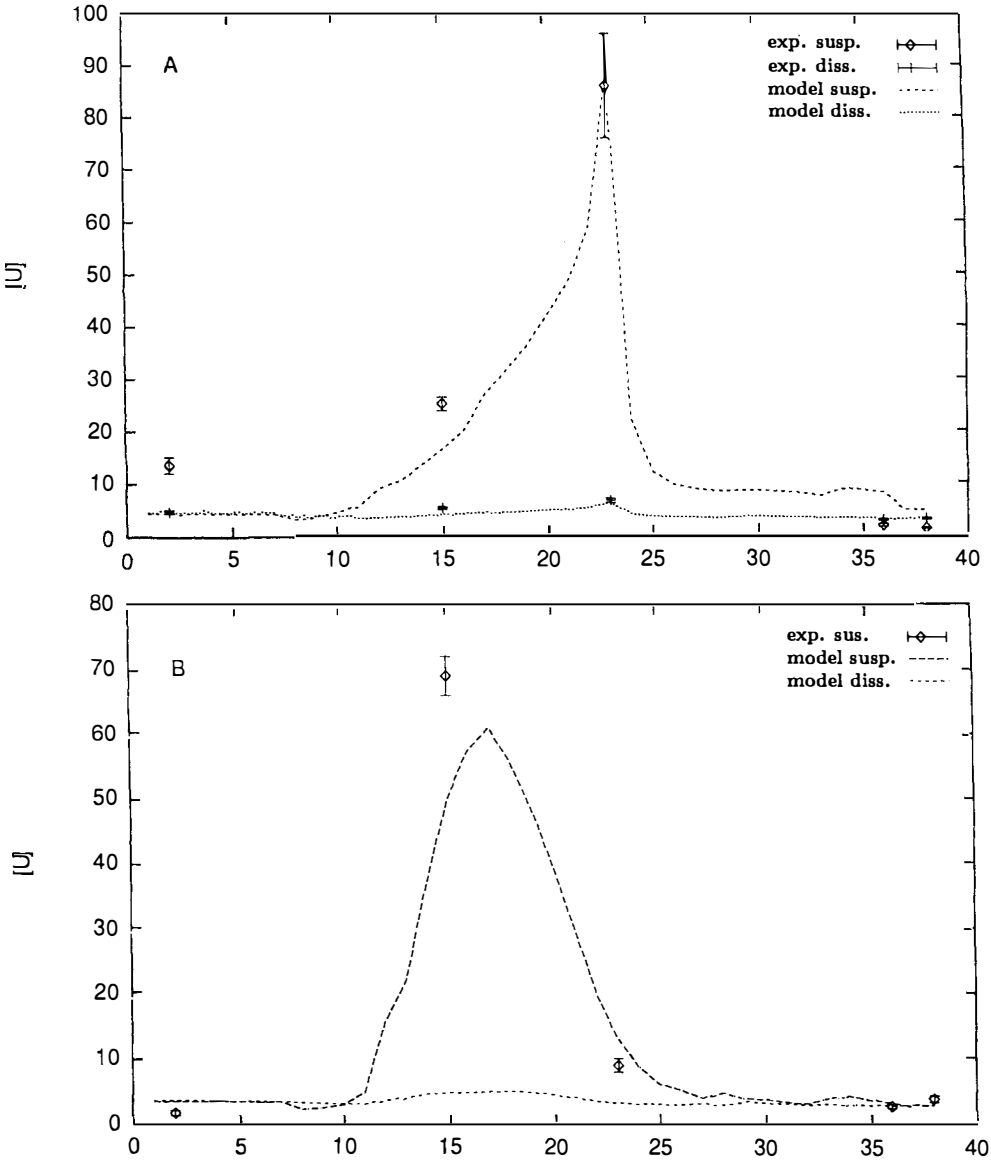

Fig. 19. Model results for U dispersion, for the low (A) and high (B) water samples. U concentrations in water are given in μg/l, and in suspended matter in μg/g.

the fact that an excess of Th has been measured in sediments collected close to the complex (Martínez-Aguirre et al., 1994a).

The model sensitivity to the different parameters, the way of creating the background and the magnitude of the source term have also been studied. These can be seen in Periáñez et al. (1994a, 1996c).

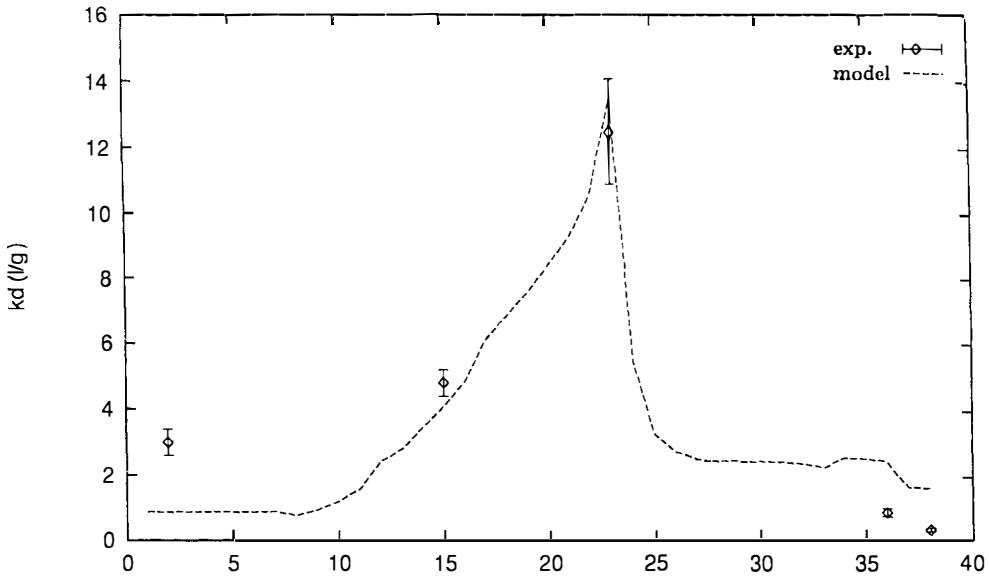

Fig. 20. Computed and measured distribution coefficients (l/g) for U during low water.

3.5.3. *Predictive studies*

Some predictive studies concerning the process of cleaning of the estuary have been carried out with the model. ^{226}Ra was used for the numerical experiments. A simulation over 10 tidal cycles was performed, during which there were no activity discharges to the estuary. Concentrations in the sediments were those measured by Martínez-Aguirre et al. (1994a) and arbitrary, although realistic, concentrations were assumed as initial conditions for water and suspended matter. These should simulate the ^{226}Ra background remaining in the estuary after activity discharges stop.

In a first trial they were 50 mBq/l in water and 25 mBq/g in the surface layer of suspended matter particles. After the simulation, it was verified that there were no apparent changes in sediment specific activities over such a time period. Thus, the process of cleaning of the sediment should be studied with a model based upon residual circulation, that allows larger time steps and, consequently, simulations over longer time scales (years) can be carried out (Periáñez & Martínez-Aguirre, 1997b). The time evolution of computed specific activities in water and the surface layer of suspended matter particles, and distribution coefficients in a compartment of the central part of the grid can be seen in Fig. 24. Concentrations in both phases, as well as the distribution coefficient, begin to oscillate at the same frequency as tidal oscillations. It is interesting to note that specific activities increase in both phases although there are no external inputs to the estuary. This activity comes from the sediments, that now act as a source of radionuclides as they are slowly cleaned. Similar effects have been found in other modelling work (Hofer & Bayer, 1997).

These results have been obtained with arbitrary initial concentrations in water and suspended matter. The results of the same simulation, but starting from different initial conditions are presented in Fig. 25. The new initial conditions are 50 mBq/l and 100 mBq/g for water and

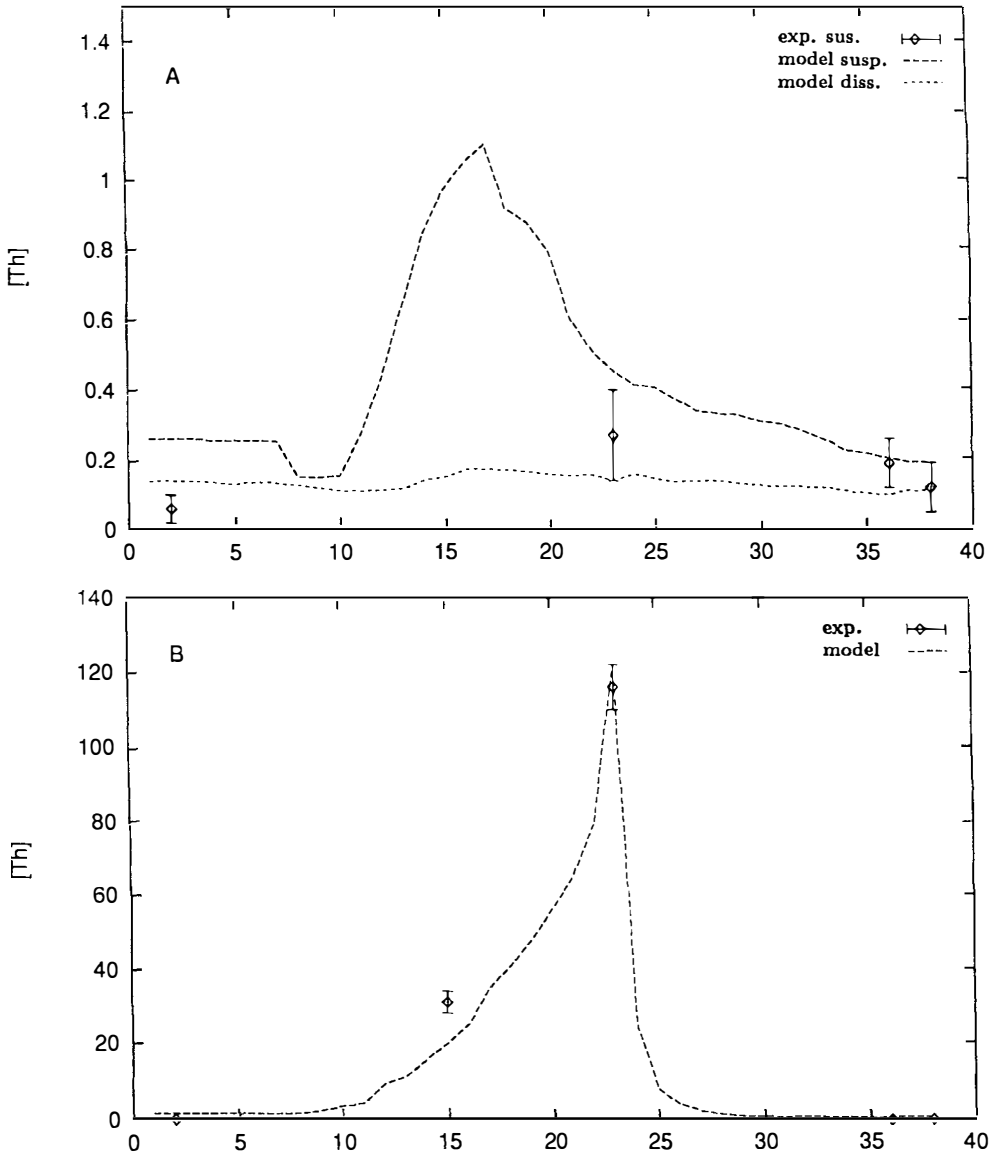

Fig. 21. Model results for Th dispersion. (A): water and suspended matter during high water. (B): suspended matter during low water. (C): water during low water. Concentrations are given in μg/l and μg/g for water and suspended matter, respectively.

the surface layer of suspended matter particles respectively. As before, specific activities and distribution coefficients oscillate following tides, and concentration in water increases again. However, it is interesting to note that at the end of the simulation, the distribution coefficient has reached the same value as in the previous case. It seems that the distribution coefficient

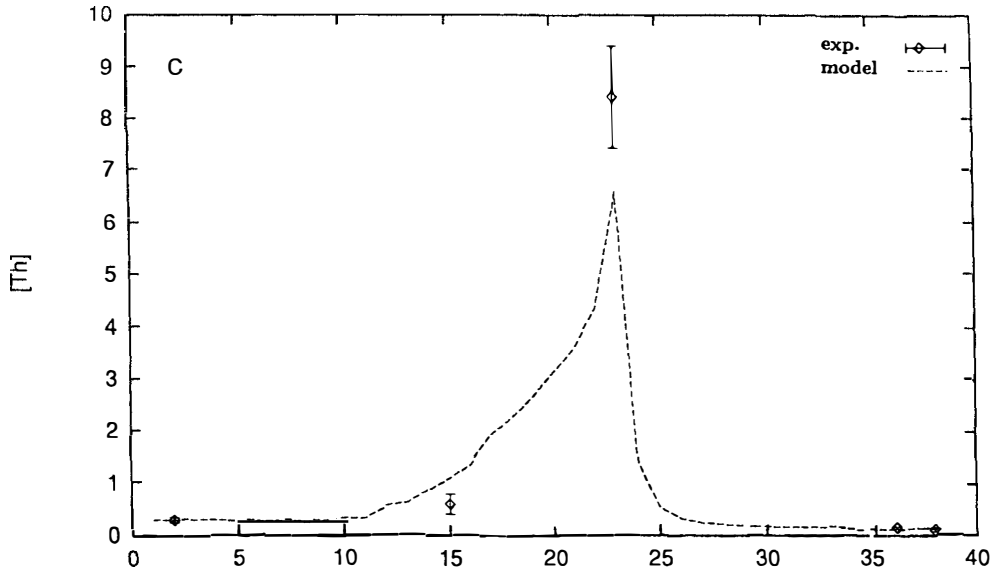

Fig. 21. (Continued).

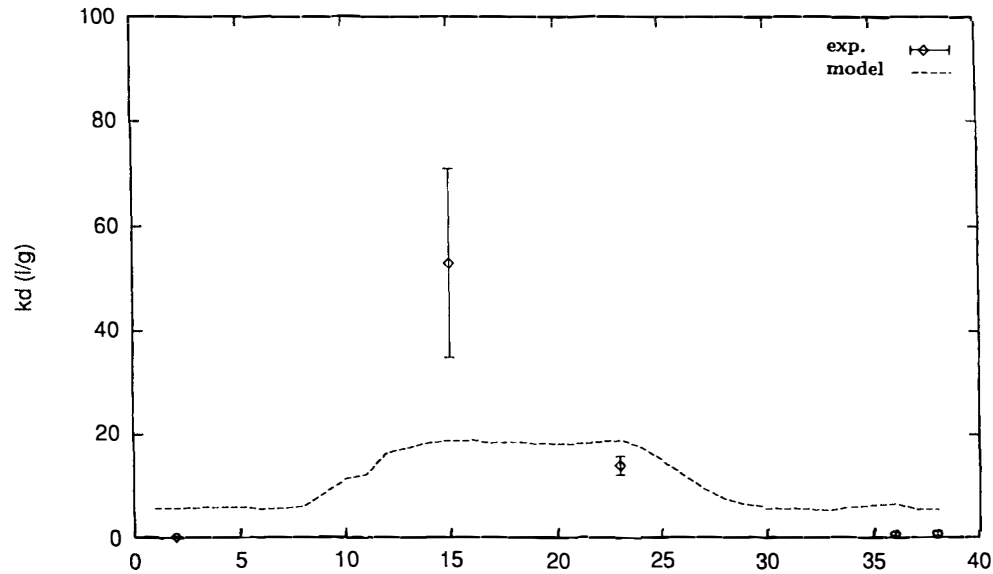

Fig. 22. Computed and measured distribution coefficients (l/g) for Th during low water.

tends to an equilibrium value (slightly altered by tidal oscillations) independently of the initial activities.

From equation (30), substituting the corresponding values of χ_1 and k_2 for ^{226}Ra, and the values selected for ρ and R, the equilibrium distribution coefficient for ^{226}Ra is $k_d = 0.52$ l/g.

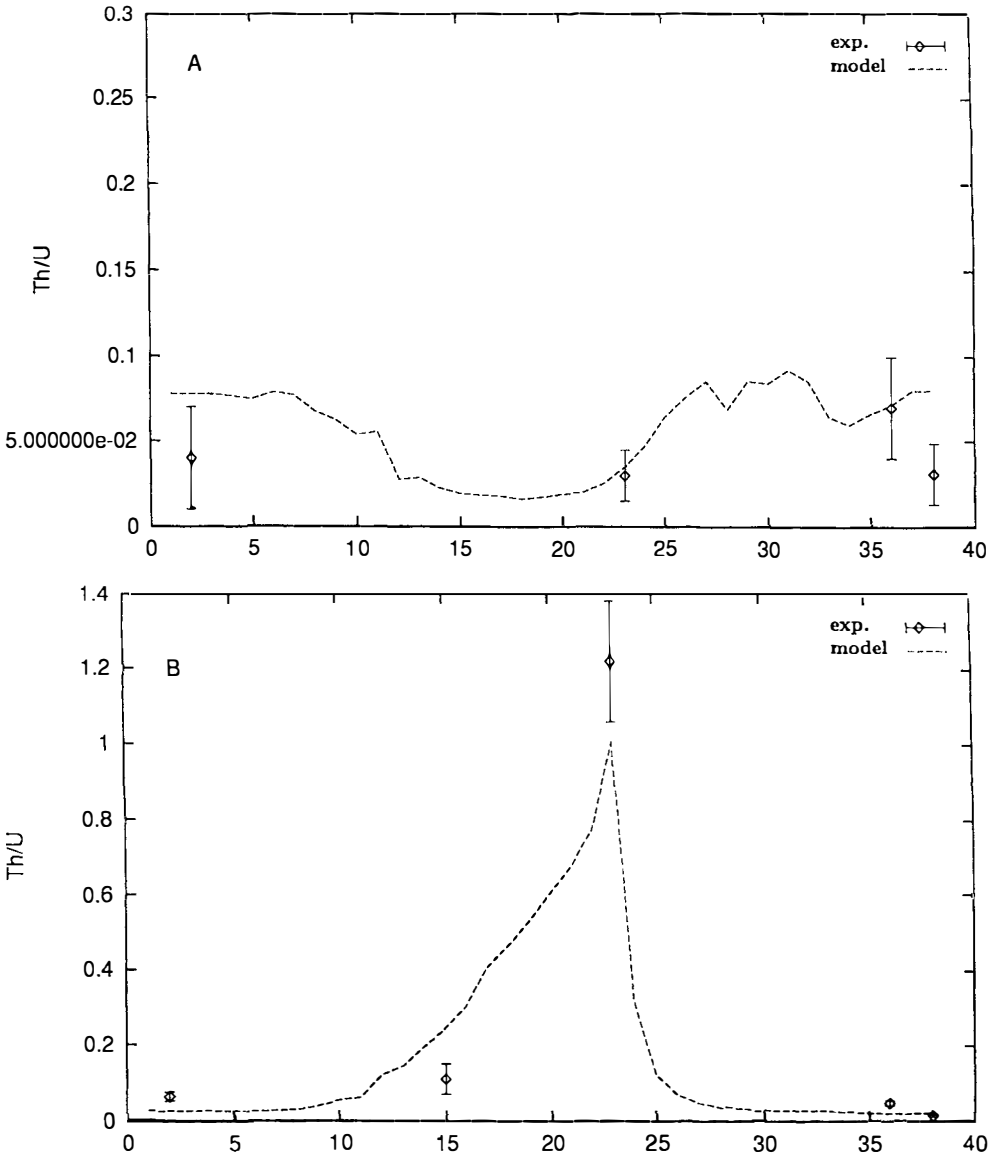

Fig. 23. Computed and measured Th/U mass ratios for suspended matter during high water (A), water samples during low water (B) and suspended matter during low water (C).

Nevertheless, ^{226}Ra is a natural radionuclide that is present in the central part of suspended particles. These radionuclides that are locked in particles cannot be exchanged with the liquid phase (and are not considered in equation (30)), but are considered when an experimental determination of k_d is carried out. The model accounts for this by assuming a background ^{226}Ra activity in the central part of particles equal to 45 mBq/g (Periáñez et al., 1996c),

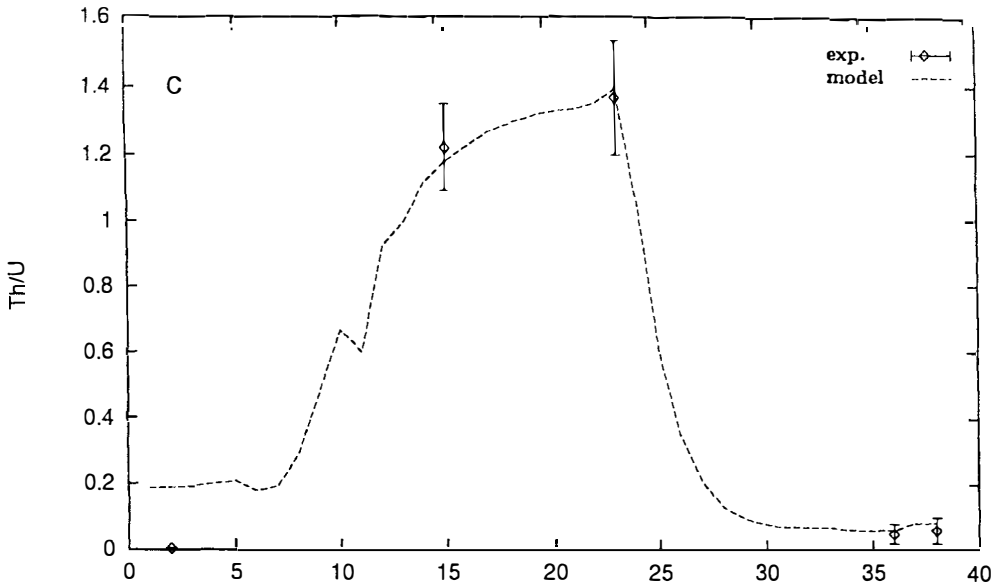

Fig. 23. (Continued).

since this is the measured specific activity in suspended matter far upstream of the fertilizer complex. Thus, the contribution of this activity to the k_d is $45/80 = 0.56$ l/g (80 is specific activity in water, Fig. 25). If this contribution is subtracted from the computed k_d, we obtain $k_d = 1.1 - 0.56 = 0.54$ l/g, which is the value that can be compared with the result obtained from equation (30), 0.52 l/g. Therefore, it can be concluded that after the simulation time, the transfers between water and suspended matter have reached equilibrium (slightly altered by tidal oscillations, as mentioned above). Moreover, equilibrium k_d, 1.1 l/g, agrees with that defined in current literature. Indeed, it can be seen in IAEA (1985) that ^{226}Ra k_d in coastal waters ranges from 0.5 to 50 l/g, with a mean value of 5 l/g.

4. Conclusions of the chapter

The dispersion of radionuclides in an estuarine system has been studied. The Odiel river estuary, located at the southwest of Spain, forms a fully mixed estuary in which M_2 is the main tidal constituent. A phosphate fertilizer processing complex releases its wastes to the estuary, thus leading to clearly enhanced levels of natural radionuclides in water, suspended matter and sediments.

The physical characteristics of the estuary defines the model to be applied. In this case, a 1D model has been used to study the general aspects of the movement of dissolved radionuclides in the estuary. Also, a 2D depth averaged model has been applied to study, in detail, the dispersion of non conservative radionuclides in the area close to the release point from the complex. The transfers of radionuclides between the liquid and solid phases have been described in terms of kinetic transfer coefficients. The model must solve, together with the

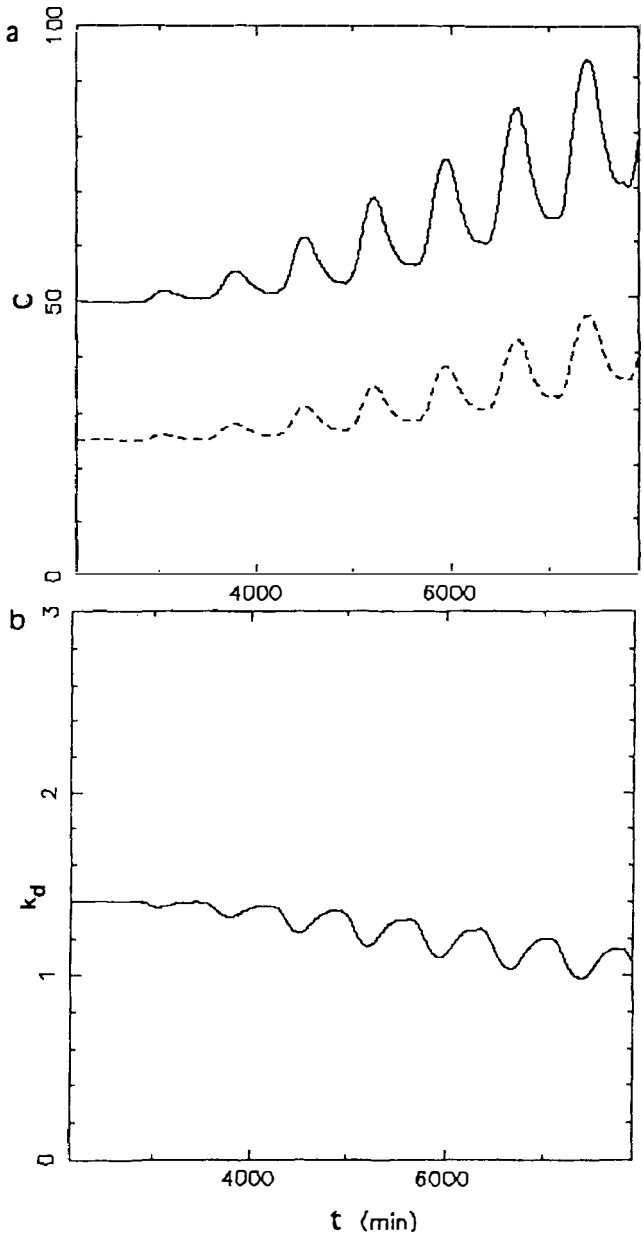

Fig. 24. (a) Time evolution of ^{226}Ra concentrations in water, in mBq/l (solid line), and in the surface layer of suspended matter, in mBq/g (dashed line), for a cell in the center of the grid. (b) Time evolution of the distribution coefficient (l/g) in the same grid cell.

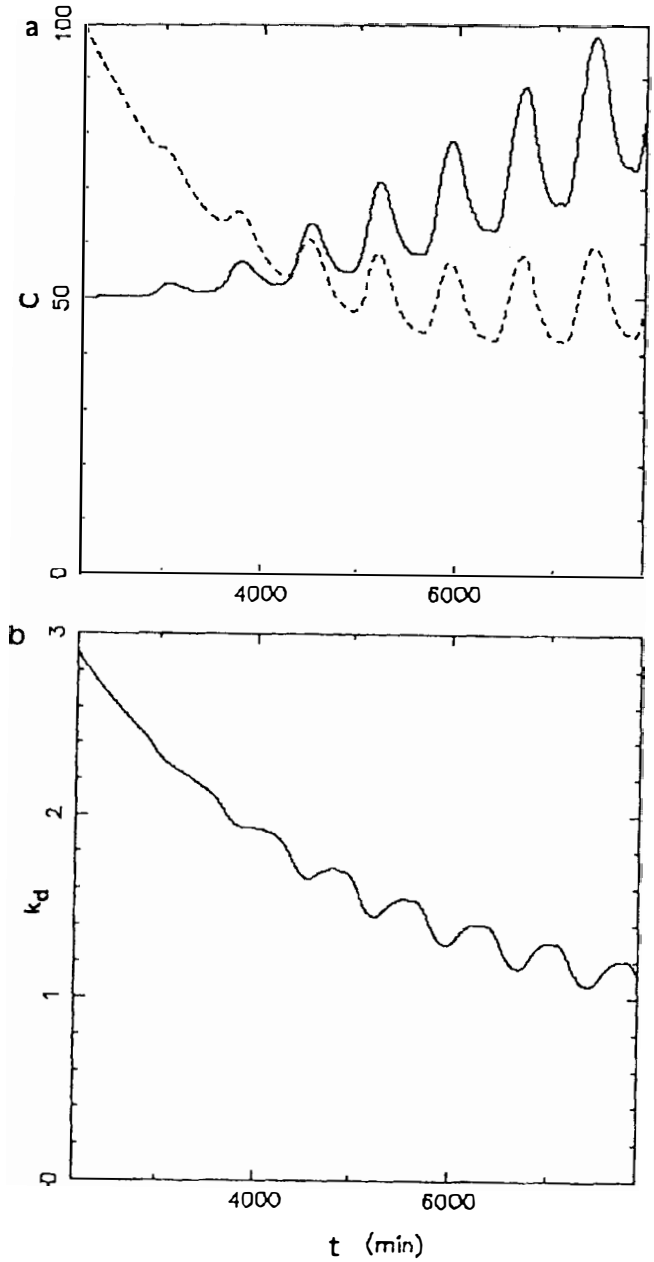

Fig. 25. Same as the previous figure, but starting from different concentrations in water and in the surface layer of suspended matter particles.

equations whose solutions give the time evolution of specific activities in each of the four phases considered in the model, the hydrodynamic equations and the suspended matter equation, including the erosion and deposition terms.

This model has been applied to simulate the dispersion of ^{226}Ra, ^{238}U and ^{232}Th. In general, the model reproduces the behaviour of these radionuclides in the estuary. Computed k_d are also, in general, in agreement with measurements. It has also been observed that cleaning of the estuary is a slow process since the sediments act as a source of radionuclides to the water column once that direct discharges from the fertilizer complex have stopped.

Finally, it should be pointed out that these kind of models are useful predictive tools that can be used in the assessment of contamination (radioactive, heavy metals, chemicals) following accidental or deliberate releases. Also, due to the predictive possibilities of the models, they can be applied for engineering purposes, to investigate, for instance, the effect of a potential dredging in the movement of a contaminated sediment.

Acknowledgements

Work supported by ENRESA and contracts DGICYT PB89-0621, EU FI3P-CT92-0035 and DGESIT 1FD97-0900-C02-01. The authors are also indebted to Prof. M. García-León for his careful reading of the manuscript and useful suggestions to improve it.

References

Abril, J. M. & Abdel-Aal, M. M. (2000). Marine Radioactivity Studies in the Suez Canal, Part I: Hydrodynamics and Transit Times. *Estuarine, Coastal and Shelf Science, 50*, 489–502.

Abril, J. M., Abdel-Aal, M. M., Al-Gamal, S. A., Abdel-Hay, F. A. & Zahar, H. M. (2000). Marine Radioactivity Studies in the Suez Canal, Part II: Field experiments and a Modelling Study of Dispersion. *Estuarine, Coastal and Shelf Science, 50*, 503–514.

Aldridge, J. N. (1998). A model for prediction of marine radionuclide transport in both particulate and dissolved phases. *Radiation Protection Dosimetry, 75*, 99–103.

Baver, L. D., Gardner, W.H . & Gardner, W. R. (1992). *Soil Physics*, New York: Wiley.

Belderson, R. H. (1964). Holocene sedimentation in the western half of the Irish Sea. *Marine Geology, 2*, 147–163.

Benes, P. & Cernik, M. (1992). Kinetics of radionuclide interaction with suspended solids in modelling the migration of radionuclides in rivers. Effect of the concentration of solids and temperature. *Journal of Radioanalytical Nuclear Chemistry, Articles, 159*, 187–200.

Benes, P., Cernik, M. & Lam-Ramos, P. (1992). Factors affecting interaction of radiocesium with freshwater solids. Contact time, concentration of solids and temperature. *Journal of Radioanalytical Nuclear Chemistry, Articles, 159*, 201–218.

Bolivar, J. P. (1995). Aplicaciones de la espectrometría gamma y alfa al estudio del impacto radiactivo producido por industrias no nucleares. PhD Thesis, University of Seville (in Spanish).

Borrego, J. & Pendon, J. G. (1988). Algunos ejemplos de influencia de los procesos antrópicos en el medio sedimentario: la ría de Huelva. *Henares, Revista de Geología, 2*, 299–305 (in Spanish).

Clarke, S. (1995). *Advective/diffusion processes in the Firth of Forth. PhD Thesis.* Bangor: University of Wales.

Eisma, D. (1981). Supply and deposition of suspended matter in the North Sea. *Spec. Publs. int. Ass. Sediment, 5*, 515–428.

Eisma, D. (1993). *Suspended matter in the aquatic environment.* Berlin: Springer.

Flather, R. A. & Heaps, N. S. (1975). Tidal computations for Morecambe Bay. *Geophysical Journal of the Royal Astronomical Society, 42*, 489–517.

French, R. H. (1985). *Hidráulica de canales abiertos*, México: McGraw Hill (in Spanish).

Heijde, H. B. van, Klijn, P. J. & Passchier, W. F. (1988). Radiological impacts of the disposal of phosphogypsum. *Radiation Protection Dosimetry, 24*, 419–423.

Hofer, H. & Bayer, A. (1997). Assessment of the dispersion of radionuclides in flowing water using a dynamic model. In G. Desmet, R. J. Blust, R. N. J. Comans, J. A. Fernandez, J. Hilton & A. de Bettencourt (Eds), *Freshwater and estuarine radioecology* (pp. 489–496). Amsterdam: Elsevier.

IAEA (1985). Sediment k_d and concentration factors for radionuclides in the marine environment. *Technical Reports Series, 247*, Vienna.

IHM (1992). *Anuario de mareas 1993*. Cádiz: Instituto Hidrográfico de la Marina, Sección Oceanográfica (in Spanish).

Irving, S. H. (1978). *Mecánica de Fluidos*. México: McGraw Hill (in Spanish).

Kowalick, Z. & Murty, T. S. (1993). *Numerical modelling of ocean dynamics*. Singapore: World Scientific.

Laiche, T. P. & Scott, L. M. (1991). A radiological evaluation of phosphogypsum. *Health Physics, 60*, 691–693.

Laissaoui A. (1999). Estudios sobre los procesos que regulan el comportamiento de los radionúclidos en aguas de estuario. Aplicación a la Ría de Huelva. PhD Thesis. University of Seville (in Spanish).

Laissaoui A., Abril, J. M., Periáñez, R., García-León, M. & García-Montaño, E. (1998). Kinetic transfer coefficients for radionuclides in estuarine waters: reference values from ^{133}Ba and effect of salinity and suspended load concentration. *Journal of Radionalytical Nuclear Chemistry, Articles, 237*, 55–61.

Li, Y. H., Burkhardt, L., Buchholtz, M., O'Hara, P. & Santschi, P. H. (1984). Partition of radiotracers between suspended particles and seawater. *Geochimica and Cosmochimica Acta, 48*, 2011–2019.

Margvelashvily, N., Maderick, V. & Zheleznyak, M. (1997). THREETOX: a computer code to simulate three dimensional dispersion of radionuclides in stratified water bodies. *Radiation Protection Dosimetry, 73*, 177–180.

Martínez-Aguirre, A., García-León. M. & Ivanovich, M. (1994a). The distribution of U, Th and ^{226}Ra derived from the phosphate fertilizer industries on an estuarine system in southwest Spain. *Journal of Environmental Radioactivity, 22*, 155–177.

Martínez-Aguirre, A., García-León, M. & Ivanovich, M. (1994b). U and Th distribution in solution and suspended matter from rivers affected by phosphate rock processing in southwestern Spain. *Nuclear Instruments and Methods, A339*, 287–293.

Mehta, A. J. (1989). On estuarine cohesive sediment suspension behaviour. *Journal of Geophysical Research, 94* (C10), 14303–14314.

Nyffeler, U. P., Li, Y. H. & Santschi P. H. (1984). A kinetic approach to describe trace-element distribution between particles and solution in natural aquatic systems. *Geochimica and Cosmochimica Acta, 48*, 1513–1522.

Pejrup, M. (1988). Suspended sediment transport across a tidal flat. *Marine Geology, 82*, 187–198.

Periáñez, R. (1995). Un modelo matemático para la simulación de la dispersión de radionúclidos no conservativos en un sistema estuario. Aplicación a la ría de Huelva. PhD Thesis, University of Seville (in Spanish).

Periáñez, R. (1999). Three dimensional modelling of the tidal dispersion of non conservative radionuclides in the marine environment. Application to ^{239,240}Pu dispersion in the eastern Irish Sea. *Journal of Marine Systems, 22*, 37–51.

Periáñez, R. (2000a). Modelling the tidal dispersion of ^{137}Cs and ^{239,240}Pu in the English Channel. *Journal of Environmental Radioactivity, 49*, 259–277.

Periáñez, R. (2000b). Modelling the physico-chemical speciation of plutonium in the eastern Irish Sea. *Journal of Environmental Radioactivity, 49*, 11–34.

Periáñez, R. & García-León M. (1993). Ra-isotopes around a phosphate fertilizer complex in an estuarine system at the southwest of Spain. *Journal of Radioanalytical and Nuclear Chemistry, Articles, 172*, 71–79.

Periáñez, R. & Martínez-Aguirre, A. (1997a). Uranium and thorium concentrations in an estuary affected by phosphate fertilizer processing: experimental results and a modelling study. *Journal of Environmental Radioactivity, 35*, 281–304.

Periáñez, R. & Martínez-Aguirre, A. (1997b). A six phases model to simulate the contamination by non conservative radionuclides of sediments, soils and plants in a marsh area. Application to the Odiel Marsh in southwest Spain. *Journal of Environmental Radioactivity, 37*, 29–54.

Periáñez, R., Abril, J.M. & García-León, M. (1994a). A modelling study of ^{226}Ra dispersion in an estuarine system in southwest Spain. *Journal of Environmental Radioactivity, 24*, 159–179.

Periáñez, R., García-León, M. & Abril, J. M. (1994b). Radium isotopes in suspended matter in an estuarine system at the southwest of Spain. *Journal of Radioanalytical and Nuclear Chemistry, Articles, 183*, 395–407.

Periáñez, R., Abril, J. M. & García-León, M. (1996a). Modelling the suspended matter distribution in an estuarine system. Application to the Odiel river in southwest Spain. *Ecological Modelling, 87*, 169–179.

Periáñez, R., Abril, J. M. & García-León, M. (1996b). Modelling the dispersion of non conservative radionuclides in tidal waters. Part 1: conceptual and mathematical model. *Journal of Environmental Radioactivity, 31*, 127–141.

Periáñez, R., Abril, J. M. & García-León, M. (1996c). Modelling the dispersion of non conservative radionuclides in tidal waters. Part 2: application to ^{226}Ra dispersion in an estuarine system. *Journal of Environmental Radioactivity, 31*, 253–272.

Periáñez, R., Martínez-Aguirre, A. & García-León, M. (1996d). U and Th isotopes in an estuarine system in southwest Spain: tidal and seasonal variations. *Applied Radiation and Isotopes, 47*, 1121–1125.

Plata, A. (1985). *Dispersión en ríos*. Madrid: CEDEX (in Spanish).

Postma, H. (1980). Sediment transport and sedimentation. In E. Olausson & I. Cato (Eds), *Chemistry and biogeochemistry of estuaries* (pp. 153–186). New York: Wiley.

Prandle, D. (1974). A Numerical Model of the Southern North Sea and River Thames. Report 4. Bidston, U.K.: Institute of Oceanographic Sciences.

Prandle, D. (1984). A modelling study of the mixing of ^{137}Cs in the seas of the European continental shelf. *Philosophical Transactions of the Royal Society, London, A310*, 407–436.

Prandle, D., Jago, C. F., Jones, S. E., Purdie, D. A. & Tappin, A. (1993). The influence of horizontal circulation in the supply and distributions of tracers. *Philosophical Transactions of the Royal Society, London, A343*, 405–421.

Pugh, D. T. (1987). *Tides, surges and mean sea level*. Chichester: Wiley.

Universidad de Sevilla (1991). Coeficientes de distribución de radionucleidos. Contract with ENRESA, Final Report (in Spanish).

Williams, J. J., Humphery, J. D., Hardcastle, P. J. & Wilson, D. J. (1998). Field observations of hydrodynamic conditions and suspended particulate matter in the southern North Sea. *Continental Shelf Research, 18*, 1215–1233.